

The information about the state of a qubit gained by a weakly coupled detector

S Ashhab^{1,2,4}, J Q You^{1,3} and Franco Nori^{1,2}

¹ Advanced Science Institute, The Institute of Physical and Chemical Research (RIKEN), Wako-shi, Saitama 351-0198, Japan

² Physics Department, Michigan Center for Theoretical Physics, The University of Michigan, Ann Arbor, Michigan 48109-1040, USA

³ Department of Physics and Surface Physics Laboratory (National Key Laboratory), Fudan University, Shanghai 200433, People's Republic of China

E-mail: ashab@riken.jp

New Journal of Physics **11** (2009) 083017 (35pp)

Received 11 May 2009

Published 13 August 2009

Online at <http://www.njp.org/>

doi:10.1088/1367-2630/11/8/083017

Abstract. We analyze the information that one can learn about the state of a quantum two-level system, i.e. a qubit, when probed weakly by a nearby detector. In particular, we focus on the case when the qubit Hamiltonian and the qubit's operator being probed by the detector do not commute. Because the qubit's state keeps evolving while being probed and because the measurement data is mixed with detector-related background noise, one might expect the detector to fail in this case. We show, however, that under suitable conditions and by proper analysis of the measurement data useful information about the state of the qubit can be extracted. It turns out that the measurement basis is stochastically determined every time the experiment is repeated. We analyze in detail the probability distributions that govern the choice of measurement bases. We also analyze the information acquisition rate and show that it is largely unaffected by the apparent conflict between the measurement and intrinsic qubit dynamics. We discuss the relation between our analysis and the stochastic master equation that describes the evolution of the qubit's state under the influence of measurement and decoherence. In particular, we write down a stochastic equation that encompasses the usual stochastic master equation for the evolution of the qubit's density matrix and additionally contains the measurement information that can be extracted from the observed signal.

⁴ Author to whom any correspondence should be addressed.

Contents

1. Introduction	2
2. Model	4
3. Measurement- and Hamiltonian-induced dynamics	6
3.1. Short-time evolution	6
3.2. Extracting information from the matrix $\hat{U}_{\text{Total}}[I(t:0 \rightarrow t_f), \delta I, \delta t]$	8
3.3. Incorporating the matrix $\hat{U}_{\text{Total}}[I(t:0 \rightarrow t_f), \delta I, \delta t]$ into the formalism of stochastic master equations	10
4. Numerical results and discussion	11
4.1. Stochastically determined measurement basis	12
4.2. Information acquisition rate	14
4.3. The information contained in the QPC's output signal	15
4.4. Spectral analysis of the measurement-basis probability distribution	15
4.5. Short-time dynamics	16
4.6. Alternative interpretation: choosing the measurement basis independently of the measurement outcome	18
4.7. Small-current case	20
4.8. Quantum state tomography	22
5. Decoherence	23
6. Conclusion	27
Acknowledgments	28
Appendix A. The QPC-current probability distribution for a short time interval of size δt	28
Appendix B. The relation between a given output signal and its 'opposite'	29
Appendix C. The measurement fidelity for two consecutive weak measurements	31
Appendix D. Quantum state tomography	33
References	34

1. Introduction

Quantum measurement is a subject of importance both as a central part of quantum theory [1] and for its relevance to quantum information theory [2]. At the most basic level, the measurement is commonly thought of as a sudden projective operation that leaves the measured system in an eigenstate of the probed operator. It should be kept in mind, however, that the measurement process is a physical process that follows from a physical interaction between the measured system and the measuring device. As a result, any realistic measurement is carried out over a finite duration. One can therefore have the situation where the measurement process occurs concurrently with other physical processes. This is the situation that we consider in this paper.

Although the analysis and results of this paper should be valid for a variety of different physical settings, we find it useful to formulate the analysis in terms of a specific setup. In this paper, we use the example of a double-quantum-dot charge qubit that is probed by a quantum

point contact (QPC) [3]–[14]^{5,6}. The principle of the measurement is the fact that the current in the QPC is sensitive to the charge state of the qubit. By measuring the current passing through the QPC, one can infer the state of the qubit. One limitation that arises in practical situations is that, in order to minimize the effects of the detector on the qubit at times when no measurement is performed (e.g. during the implementation of quantum gates), the qubit–detector coupling is set to a value that is small compared to the qubit’s energy scale. As a result one must deal with some form of weak-measurement regime. This type of weak, charge-sensitive readout works well when the qubit is biased such that the charge states are eigenstates of the Hamiltonian and therefore do not mix during the measurement. In this case one can allow the detector to probe the qubit for as long as is needed to obtain a high signal-to-noise ratio, without having to worry about any intrinsic qubit dynamics.

In contrast to the simple situation described above, when the detector weakly probes the charge state of the qubit, while the Hamiltonian induces mixing dynamics between charge states, it becomes unclear how to interpret a given measurement signal. Given the fact that the signal typically contains a large amount of detector-related noise and the measurement causes unavoidable relaxation in the qubit, it might seem that this type of measurement cannot be used to determine the initial state of the qubit, i.e. at the time that the experimenter decides to perform the measurement. Indeed, there have been a number of studies analyzing the measurement-induced decoherence and the evolution of the qubit’s state in this situation [3]–[8], [14], but not the question of how to take the measurement data and extract from it information about the initial state of the qubit. This question is a key issue for qubit-state readout and is the main subject of this paper.

We shall show below that high-fidelity measurement information can be extracted from the measurement data, provided that additional decoherence mechanisms are weak and the readout signal can be monitored at a sufficiently short timescale. It turns out that not only the measurement result but also the measurement basis is determined stochastically in this case. In spite of the uncontrollability of the measurement basis, the measurement results contain meaningful information about the initial state of the qubit. In order to demonstrate this statement, we show how these results can be used to perform quantum state tomography on the qubit. These results show that under suitable conditions and by proper analysis of the measurement data useful information about the state of the qubit can be extracted from this data.

This paper is organized as follows: In section 2, we introduce the theoretical model for describing a charge qubit probed by a QPC. In section 3, we formulate the theoretical framework for the qubit evolution conditioned on the QPC’s output signal and how measurement information can be extracted from this signal. We also introduce an equation that supplements the stochastic master equation for purposes of interpreting the measured QPC signal. In section 4, we present results of numerical calculations that display a number of interesting results in this system, most importantly the stochastic nature of the measurement basis and the near-independence of the measurement fidelity from the relation between the charge basis and energy eigenbasis. In section 5, we discuss how decoherence can be introduced to the problem and how one should interpret the measurement data in the presence of decoherence. We analyze one simple example that shows how the measurement data recorded at later times

⁵ We shall not consider measurement methods based on probing the capacitance of the qubit [15].

⁶ A new measurement mechanism in this system was also proposed in [16].

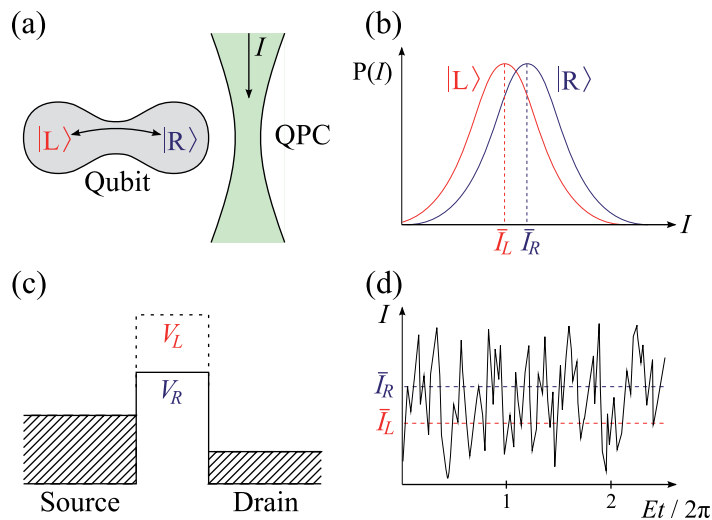


Figure 1. Schematic diagrams of (a) a charge qubit with charge states $|L\rangle$ and $|R\rangle$ measured by a QPC, (b) the probability distributions of the possible QPC current values for the two charge states of the qubit, (c) the filled energy levels of the QPC's electrodes and the energy barriers for tunneling between the electrodes for the two charge states of the qubit and (d) a typical QPC current signal. The finite widths of the probability distributions in (b) are a result of the finite measurement time. When the distance between the two center points, $|\bar{I}_R - \bar{I}_L|$, is much smaller than the widths of the distributions, the QPC performs a weak measurement on the qubit in the short interval under consideration (i.e. the time interval for which these probability distributions are relevant). The fast fluctuations in (d) convey the assumption that these fluctuations have a much shorter timescale than the qubit's precession period. In plotting (b)–(d), we have assumed that $\bar{I}_R > \bar{I}_L$, which would be the case if the qubit is defined by an extra positive charge (e.g. a hole) tunneling between the two wells. Taking the opposite case, i.e. $\bar{I}_L > \bar{I}_R$, would only result in a few sign changes in the analysis below. The main results are not affected by this choice.

is less 'valuable' than that recorded at earlier times. Concluding remarks are given in section 6. Some details of the calculations are given in the appendices.

2. Model

We consider a system composed of a charge qubit capacitively coupled to a QPC, as illustrated in figure 1. The qubit can be viewed as a system where a charged particle is trapped in a double-well potential and can occupy and tunnel between the localized ground states of the two wells. We shall denote these states by $|L\rangle$ and $|R\rangle$.

During the measurement a voltage is applied to the QPC, and a current flows through it. Except for the discussion given in section 5, we shall assume that the QPC does not induce any qubit decoherence except that associated with the measurement-induced projection. Before analyzing the general case, we first consider the case where the qubit Hamiltonian is diagonal

in the charge basis. In this case, there is no mechanism by which the states $|L\rangle$ and $|R\rangle$ mix during the system dynamics. As a result, if the qubit is initially in the state $|L\rangle$, the long-time-averaged QPC current will be given by \bar{I}_L , and the qubit will remain in the state $|L\rangle$. A similar statement applies to the state $|R\rangle$ of the qubit, with corresponding QPC current \bar{I}_R . The QPC current therefore serves as an indicator of the qubit's state in the charge basis $\{|L\rangle, |R\rangle\}$, as long as the qubit Hamiltonian does not mix the states of this basis.

On any finite timescale, there will be fluctuations in the QPC current, and the observed value might deviate from \bar{I}_L or \bar{I}_R . The longer the period over which the averaging is made, the smaller the fluctuations. One can therefore define a measurement timescale that determines how long one needs to wait in order to distinguish between the states $|L\rangle$ and $|R\rangle$. The relation between this timescale and the qubit's Hamiltonian-induced precession period separates two measurement regimes: strong and weak qubit-detector coupling. As mentioned above, this separation is irrelevant when the qubit Hamiltonian is diagonal in the charge basis.

For the remainder of this paper, we analyze the general case where the qubit Hamiltonian is not necessarily diagonal in the charge basis. The Hamiltonian of the combined qubit+QPC system can be expressed as

$$\hat{H} = \hat{H}_q + \hat{H}_{\text{QPC}} + \hat{H}_{\text{int}}. \quad (1)$$

In describing the qubit, we shall use the eigenbasis of the qubit Hamiltonian \hat{H}_q . Thus \hat{H}_q can be expressed as

$$\hat{H}_q = \begin{pmatrix} -\frac{E}{2} & 0 \\ 0 & \frac{E}{2} \end{pmatrix} = -\frac{E}{2} \hat{\sigma}_z, \quad (2)$$

where E is the energy splitting between the qubit's two energy levels and $\hat{\sigma}_z$ is the z -axis Pauli matrix. We shall express the ground and excited states of the Hamiltonian as $|0\rangle$ and $|1\rangle$, respectively. The electric dipole moment operator $|R\rangle\langle R| - |L\rangle\langle L|$ can be expressed as $\hat{\sigma}_{\mathbf{n}}$, where \mathbf{n} is a vector that represents the direction of the charge basis relative to the energy eigenbasis:

$$\begin{aligned} \hat{\sigma}_{\mathbf{n}} &= |R\rangle\langle R| - |L\rangle\langle L| \\ &= \cos \beta \hat{\sigma}_z + \sin \beta \hat{\sigma}_x, \end{aligned} \quad (3)$$

where β represents the angle between the charge basis and the energy eigenbasis. The states of the charge basis (i.e. the eigenstates of $\hat{\sigma}_{\mathbf{n}}$) can be expressed as

$$\begin{aligned} |R\rangle &= \cos \frac{\beta}{2} |0\rangle + \sin \frac{\beta}{2} |1\rangle, \\ |L\rangle &= \sin \frac{\beta}{2} |0\rangle - \cos \frac{\beta}{2} |1\rangle. \end{aligned} \quad (4)$$

The QPC Hamiltonian \hat{H}_{QPC} can be expressed as

$$\hat{H}_{\text{QPC}} = \sum_m \epsilon_{S,m} \hat{a}_m^\dagger \hat{a}_m + \sum_n \epsilon_{D,n} \hat{b}_n^\dagger \hat{b}_n + \sum_{\substack{\{m,n\} \in \\ \text{tunneling} \\ \text{channels}}} J_{m,n} \left(\hat{b}_n^\dagger \hat{a}_m + \hat{a}_m^\dagger \hat{b}_n \right), \quad (5)$$

where the operators \hat{a}_m and \hat{b}_n , respectively, annihilate electrons in the source and drain electrodes of the QPC, \hat{a}_m^\dagger and \hat{b}_n^\dagger are their hermitian conjugates, $\epsilon_{S,m}$ and $\epsilon_{D,n}$ are the energies of

single-particle quantum states in the source and drain electrodes, and $J_{m,n}$ represents tunneling matrix elements between the two electrodes. We take the qubit-QPC interaction Hamiltonian to be of the form [3]

$$\hat{H}_{\text{int}} = \hat{\sigma}_{\mathbf{n}} \sum_{\substack{\{m,n\} \in \\ \text{tunneling} \\ \text{channels}}} \delta J_{m,n} \left(\hat{b}_n^\dagger \hat{a}_m + \hat{a}_m^\dagger \hat{b}_n \right), \quad (6)$$

such that the tunneling matrix elements (and therefore the QPC current) depend on the state of the qubit in the charge basis. The QPC and its operation are illustrated in figures 1(b)–(d). When J and δJ are independent of m and n , the microscopic degrees of freedom of the QPC are not affected by, and therefore do not carry any information about, the state of the qubit. This information is carried only by the total number of electrons that have tunneled through the QPC. In the remainder of this paper, we shall assume that this is the case. We close this section by mentioning that the above description of the microscopic structure of the QPC is not needed for the analysis below, provided one accepts the description of the QPC operation explained in section 3 as a phenomenological model of the detector. Indeed, the analysis below is not restricted to the case of a charge qubit probed by a QPC.

3. Measurement- and Hamiltonian-induced dynamics

In this section, we introduce the theoretical framework for analyzing the qubit state evolution and interpreting the observed measurement data.

3.1. Short-time evolution

We start our analysis by considering a short time interval between times t and $t + \delta t$. For definiteness, we assume that during this time interval a large number of electrons tunnel through the QPC, such that it is natural to define a QPC current $I(t)$ during this short interval (the current would be defined as the amount of charge that has passed through the QPC divided by δt ; the small-current case will be discussed in section 4.6). We also assume that a weak-coupling regime exists for a properly chosen value of δt , which means that the QPC-current probability distributions (for the states $|L\rangle$ and $|R\rangle$) are broad and almost completely overlap, as shown in figure 1(b). The coherence time of the QPC and the time resolution of the QPC's output signal are both assumed to be much shorter than the precession period of the qubit. As a result, for a properly chosen value of δt one can treat the different time intervals as independent measurement processes, with each measurement being made in the charge basis.

As explained in appendix A, the QPC-current probability distribution for the qubit state $|L\rangle$ can be expressed as

$$P_L[I, \delta I, \delta t] = \sqrt{\frac{2\delta t (\delta I)^2}{\pi \tau_m (\Delta \bar{I})^2}} \exp \left\{ -\frac{2\delta t (I - \bar{I}_L)^2}{\tau_m (\Delta \bar{I})^2} \right\}, \quad (7)$$

and a similar expression can be derived for the qubit state $|R\rangle$. Here we have defined a number of useful quantities: δI is the size of a finite interval of QPC currents that we identify with a single value. One could say that with this definition we are turning the probability distributions in figure 1(b) into histograms with discrete possible values for the current I . This definition will be

useful for both the analytic and numerical calculations below. The characteristic measurement time τ_m defines the timescale needed for the QPC output to distinguish between the states $|L\rangle$ and $|R\rangle$, and $\Delta\bar{I} = \bar{I}_R - \bar{I}_L$, where for definiteness we take $\bar{I}_R > \bar{I}_L$.

We can now construct matrices that describe the qubit-state evolution depending on the observed QPC current $I(t)$. When a given value of $I(t)$ is observed in the QPC, the density matrix $\rho_q(t)$ describing the quantum state of the qubit is projected (possibly partially) according to the observed value. This projection of the qubit's state is described by a 2×2 matrix (or propagator) that we shall call $\hat{U}_M[I(t), \delta I, \delta t]$:

$$\rho_q(t + \delta t) = \frac{1}{\text{Tr} \left\{ \hat{U}_M^\dagger[I(t), \delta I, \delta t] \hat{U}_M[I(t), \delta I, \delta t] \rho_q(t) \right\}} \hat{U}_M[I(t), \delta I, \delta t] \rho_q(t) \hat{U}_M^\dagger[I(t), \delta I, \delta t]. \quad (8)$$

Measurement theory says that $\hat{U}_M[I(t), \delta I, \delta t]$ obeys the equation [2, 17]

$$\hat{U}_M^\dagger[I(t), \delta I, \delta t] \hat{U}_M[I(t), \delta I, \delta t] = P_L[I(t), \delta I, \delta t] |L\rangle\langle L| + P_R[I(t), \delta I, \delta t] |R\rangle\langle R|. \quad (9)$$

Since we are keeping only the fundamentally necessary terms in the projection dynamics, we ignore any unitary-transformation component in $\hat{U}_M[I(t), \delta I, \delta t]$ that does not affect equation (9). Any such component can, in principle, be determined experimentally, and it can then be incorporated into the analysis straightforwardly. Such a component could result if, for example, the different current states of the QPC have different charge distributions that act as an effective gate voltage on the charge qubit. Assuming a large overlap between the QPC-current probability distributions, we find that the matrix $\hat{U}_M[I(t), \delta I, \delta t]$ can be expressed in the form

$$\begin{aligned} \hat{U}_M[I(t), \delta I, \delta t] &= \sqrt{P_L[I(t), \delta I, \delta t]} |L\rangle\langle L| + \sqrt{P_R[I(t), \delta I, \delta t]} |R\rangle\langle R| \\ &= \left(\frac{2\delta t (\delta I)^2}{\pi \tau_m (\Delta\bar{I})^2} \right)^{1/4} \left[\exp \left\{ -\frac{\delta t [I(t) - \bar{I} + \Delta\bar{I}/2]^2}{\tau_m (\Delta\bar{I})^2} \right\} |L\rangle\langle L| \right. \\ &\quad \left. + \exp \left\{ -\frac{\delta t [I(t) - \bar{I} - \Delta\bar{I}/2]^2}{\tau_m (\Delta\bar{I})^2} \right\} |R\rangle\langle R| \right] \\ &\propto \exp \left\{ -\frac{\delta t [I(t) - \bar{I}]}{\tau_m \Delta\bar{I}} \right\} |L\rangle\langle L| + \exp \left\{ \frac{\delta t [I(t) - \bar{I}]}{\tau_m \Delta\bar{I}} \right\} |R\rangle\langle R| \\ &\approx 1 + \frac{\delta t [I(t) - \bar{I}]}{\tau_m \Delta\bar{I}} (|R\rangle\langle R| - |L\rangle\langle L|) \\ &= 1 + \frac{\delta t [I(t) - \bar{I}]}{\tau_m \Delta\bar{I}} \hat{\sigma}_z, \end{aligned} \quad (10)$$

where we have defined $\bar{I} = (\bar{I}_L + \bar{I}_R)/2$.

In addition to the measurement-induced evolution described by the matrix \hat{U}_M of equation (10), the qubit Hamiltonian induces a unitary evolution of the qubit's state. This contribution to the qubit-state evolution (over the time interval from t to $t + \delta t$) is described by the matrix

$$\hat{U}_H[\delta t] = \exp \left\{ -i\hat{H}_q \delta t \right\} \approx 1 + i\frac{E}{2} \delta t \hat{\sigma}_z. \quad (11)$$

The matrices $\hat{U}_M[I(t), \delta I, \delta t]$ and $\hat{U}_H[\delta t]$ can now be combined to give the total evolution matrix

$$\begin{aligned} \hat{U}[I(t), \delta I, \delta t] &\approx \hat{U}_M[I(t), \delta I, \delta t] \times \hat{U}_H[\delta t] \\ &\propto 1 + \frac{\delta t [I(t) - \bar{I}]}{\tau_m \Delta \bar{I}} \hat{\sigma}_n + i \frac{E}{2} \delta t \hat{\sigma}_z. \end{aligned} \quad (12)$$

Note that the high-resolution requirement in the QPC-current signal, which is one of our assumptions mentioned earlier in this section, enters in obtaining the above equation: both $\hat{U}_M[I, \delta I, \delta t]$ and $\hat{U}_H[\delta t]$ are approximately proportional to the unit matrix, with lowest-order corrections of order δt . Therefore they commute to first order in δt , and they can be treated as commuting operators when $E\delta t \ll 1$, i.e. when they both induce small changes to the quantum state of the qubit.

When a given QPC output signal $I(t)$ (starting from the initial time $t = 0$ until the final time t_f) is observed, one can take the corresponding short-time evolution matrices explained above and use them to construct the total evolution matrix $\hat{U}_{\text{Total}}[I(t : 0 \rightarrow t_f), \delta I, \delta t]$. This matrix describes the evolution of the qubit state from $t = 0$ until $t = t_f$, given that the current signal $I(t)$ was observed (with discretization parameters δI and δt). Using the unit matrix as the total evolution matrix for $t = 0$, we find that

$$\hat{U}_{\text{Total}}[I(t : 0 \rightarrow t_f), \delta I, \delta t] = \hat{U}[I(t_f - \delta t), \delta I, \delta t] \times \cdots \times \hat{U}[I(0), \delta I, \delta t]. \quad (13)$$

In section 3.2, we shall explain how measurement information can be extracted from the matrix \hat{U}_{Total} .

3.2. Extracting information from the matrix $\hat{U}_{\text{Total}}[I(t : 0 \rightarrow t_f), \delta I, \delta t]$

The evolution of the qubit state is obtained by taking into account a long sequence of weak measurements and Hamiltonian-induced unitary transformations. This long sequence of events, however, is equivalent to a simple scenario in which a single measurement is made on the qubit and the state of the qubit is rotated after the measurement. In order to obtain a quantitative description of this alternative interpretation of the measurement data, one takes the 2×2 matrix $\hat{U}_{\text{Total}}[I(t : 0 \rightarrow t_f), \delta I, \delta t]$ and divides it through a polar decomposition into two parts, a measurement matrix $\hat{U}_{\text{Meas}}[I(t : 0 \rightarrow t_f), \delta I, \delta t]$ followed by a unitary transformation $\hat{U}_{\text{Rot}}[I(t : 0 \rightarrow t_f), \delta I, \delta t]$:

$$\hat{U}_{\text{Total}}[I(t : 0 \rightarrow t_f), \delta I, \delta t] = \hat{U}_{\text{Rot}}[I(t : 0 \rightarrow t_f), \delta I, \delta t] \times \hat{U}_{\text{Meas}}[I(t : 0 \rightarrow t_f), \delta I, \delta t]. \quad (14)$$

The matrix $\hat{U}_{\text{Meas}}[I(t : 0 \rightarrow t_f), \delta I, \delta t]$ has the form

$$\hat{U}_{\text{Meas}}[I(t : 0 \rightarrow t_f), \delta I, \delta t] = \sqrt{P_1} |\psi_1\rangle \langle \psi_1| + \sqrt{P_2} |\psi_2\rangle \langle \psi_2|, \quad (15)$$

where $|\psi_1\rangle$ and $|\psi_2\rangle$ are two orthogonal states (the indices are assigned such that $P_1 \geq P_2$). In order to characterize the measurement matrix in terms of the information it provides about the state of the qubit, it is useful to consider the case where one initially has no information about this state. The qubit therefore starts in the maximally mixed state

$$\rho_{\text{max. mixed}} = \begin{pmatrix} \frac{1}{2} & 0 \\ 0 & \frac{1}{2} \end{pmatrix}. \quad (16)$$

After a measurement that produces the outcome corresponding to the matrix $\hat{U}_{\text{Meas}}[I(t : 0 \rightarrow t_f), \delta I, \delta t]$ (and ignoring the presence of the rotation matrix $\hat{U}_{\text{Rot}}[I(t : 0 \rightarrow t_f), \delta I, \delta t]$ for purposes of this argument), the qubit ends up in a state described by the density matrix

$$\rho_{\text{after Meas.}} = \frac{P_1}{P_1 + P_2} |\psi_1\rangle \langle \psi_1| + \frac{P_2}{P_1 + P_2} |\psi_2\rangle \langle \psi_2|. \quad (17)$$

This density matrix describes a statistical mixture of the states $|\psi_1\rangle$ and $|\psi_2\rangle$, with a higher probability for the former (except for the rare cases where $P_1 = P_2$). One can therefore say that, as a result of the measurement, one now knows that the qubit is more likely to be in the state $|\psi_1\rangle$ than in the state $|\psi_2\rangle$, in contrast to the complete lack of information at the initial time. The states $|\psi_1\rangle$ and $|\psi_2\rangle$ therefore represent the measurement basis that corresponds to the output signal $I(t)$. The measurement fidelity is calculated as follows [18]: let us assume that one is given a qubit that is in an unknown state, either $|\psi_1\rangle$ or $|\psi_2\rangle$. The parameters P_i are the probabilities that the outcome defined by $I(t)$, δI and δt is obtained given that the qubit was initially in the state $|\psi_i\rangle$. Upon observing this outcome, if one wants to make a guess about the state of the qubit, one would maximize the probability of making a correct guess by choosing the state $|\psi_1\rangle$. The difference between the probability of actually finding the state $|\psi_1\rangle$ and that of finding the orthogonal state $|\psi_2\rangle$ is given by

$$F = \left| \frac{P_1 - P_2}{P_1 + P_2} \right|. \quad (18)$$

This expression can therefore naturally be interpreted as the measurement fidelity.

It is worth pausing here to comment on the issue of the independence of the measurement basis from the measurement outcome. One typically thinks of the measurement basis as being determined by the experimenter when designing the experimental setup and the measurement result (i.e. +1 or -1 along the measurement axis) being determined stochastically according to the rules of quantum mechanics based on the measurement basis used in the experiment. The situation considered in this paper, however, cannot be described using this simple picture. Here we have a two-state quantum system and a measurement device that produces one of many possible outcomes, not necessarily all providing information in the same basis. In this case, the picture of the measurement basis being independent of the outcome is not valid in general. For example, it is possible in a general setting for a certain state $|\psi\rangle$ to be a possible result of the data analysis presented above, but not the state orthogonal to it. Such a situation arises in the problem analyzed in [18], and it complicates the interpretation of the measurement data. Fortunately, because in this paper we are dealing with two symmetric probability distributions (see figure 1(b)), we find that for every possible QPC signal there is an ‘opposite’ or ‘flipped’ signal, which can be obtained by taking the mirror image about the central line in figure 1(d) (this central line is defined by $\bar{I} = (\bar{I}_L + \bar{I}_R)/2$). It is not difficult to verify that if a given signal corresponds to a certain measured state $|\psi\rangle$, the ‘opposite’ signal will correspond to the orthogonal state with the same values of P_1 and P_2 (see appendix B for the full derivation). An important consequence of the above statement is that the total probability of finding one of two opposite signals is independent of the initial state of the qubit. Hence, the probability of obtaining a certain measurement basis is independent of the initial state of the qubit. This fact leads naturally to the conceptual interpretation that the measurement basis is determined according to some stochastic process, and the measurement result along that basis is made after the basis has been determined.

To summarize, the QPC's output signal can be used to derive the matrix $\hat{U}_{\text{Total}}[I(t : 0 \rightarrow t_f), \delta I, \delta t]$. This matrix can then be used to determine the measurement basis, the measurement result (i.e. ± 1 along the measurement axis), the fidelity (or in other words, the degree of certainty about the obtained measurement result) and the post-measurement rotation. Note that all the analysis above is performed independently of the initial state of the qubit. If one knows the initial state, one can use the evolution matrices in order to determine the probabilities of different outcomes, as well as the final state of the qubit after the measurement. As we shall show below, when the measurement fidelity approaches one, the final state can be determined even without any knowledge about the initial state.

It is worth mentioning here that the analysis presented above can be applied not only to qubits but also to systems with higher-dimensional Hilbert spaces. The main complication in the case of higher dimensions is that the description of the results becomes more intricate and less transparent. In this context, one can contrast the simple visualization of any qubit density matrix as a point in the so-called Bloch sphere, whereas there is no visually simple parametrization for a general density matrix of a three-state system.

3.3. Incorporating the matrix $\hat{U}_{\text{Total}}[I(t : 0 \rightarrow t_f), \delta I, \delta t]$ into the formalism of stochastic master equations

Equation (8) describes the projection of the qubit's density matrix conditioned on the observation of the QPC output $I(t)$. That equation treats the evolution as occurring in discrete steps. Constructing a master equation means taking equation (8) to first order in δt , and then taking the limit $\delta t \rightarrow 0$ in order to obtain the corresponding continuous-time differential equation [17]. One tricky point in carrying out this procedure is the fact that the stochastic quantity $I(t) - \bar{I}$ has fluctuations of size $1/\sqrt{\delta t}$:

$$\langle (I(t) - \bar{I})^2 \rangle = \frac{\tau_m (\Delta \bar{I})^2}{4\delta t}. \quad (19)$$

As a result, when keeping terms only to first order in δt , one must also keep terms containing $(\delta t)^2 \times (I(t) - \bar{I})^2$, etc. The quantity $I(t) - \bar{I}$ can be expressed as its expectation value at any given point in time, which is given by $\Delta \bar{I} \langle \hat{\sigma}_n \rangle / 2$, plus a fluctuation. It is customary to write the stochastic master equation not in terms of the current fluctuation, but rather in terms of a rescaled quantity, δW , whose standard deviation is equal to $\sqrt{\delta t}$. It then follows that δW should be defined using the relation

$$I(t) = \bar{I} + \frac{\Delta \bar{I}}{2} \langle \hat{\sigma}_n \rangle + \frac{\Delta \bar{I} \sqrt{\tau_m}}{2\delta t} \delta W. \quad (20)$$

Substituting equation (12) into equation (8) (ignoring the subscript 'M' here) and keeping terms to first order in δt , we find that

$$\rho_q(t + \delta t) = \rho_q - i\delta t \hat{H}_q \rho_q + i\delta t \rho_q \hat{H}_q + \frac{\delta W}{2\sqrt{\tau_m}} (\hat{\sigma}_n \rho_q + \rho_q \hat{\sigma}_n - 2\langle \hat{\sigma}_n \rangle \rho_q) + \frac{\delta t}{4\tau_m} (\hat{\sigma}_n \rho_q \hat{\sigma}_n - \rho_q), \quad (21)$$

where, for compactness, we have not expressed the time dependence of ρ_q explicitly on the right-hand side (in other words ρ_q should be interpreted as $\rho_q(t)$). This equation can now be rewritten in the form

$$\dot{\rho}_q = -i \left[\hat{H}_q, \rho_q \right] + \frac{\xi(t)}{2\sqrt{\tau_m}} (\hat{\sigma}_n \rho_q + \rho_q \hat{\sigma}_n - 2\langle \hat{\sigma}_n \rangle \rho_q) + \frac{1}{4\tau_m} (\hat{\sigma}_n \rho_q \hat{\sigma}_n - \rho_q), \quad (22)$$

where $\xi(t)$ is obtained by using the rescaling $\xi(t) = \delta W / \delta t$ and taking the limit $\delta t \rightarrow 0$:

$$\begin{aligned}\langle \xi(t) \rangle &= 0, \\ \langle \xi(t) \xi(t') \rangle &= \delta(t - t'),\end{aligned}\tag{23}$$

where $\delta(t - t')$ is the Dirac delta function. Equation (22) is the stochastic master equation for the system under consideration.

The question now is how the matrix $\hat{U}_{\text{Total}}[I(t : 0 \rightarrow t_f), \delta I, \delta t]$ fits into the picture of the stochastic master equation. One can derive a stochastic equation for the matrix $\hat{U}_{\text{Total}}[I(t : 0 \rightarrow t_f), \delta I, \delta t]$ by considering the change caused by a matrix of the form given in equation (12); note that the evolution of the matrix $\hat{U}_{\text{Total}}[I(t : 0 \rightarrow t_f), \delta I, \delta t]$ is governed by equation (13). One problem that arises here is that the matrix in the first line of equation (12) tends to zero when $\delta t \rightarrow 0$. Taking this limit therefore leads to ill-defined quantities. In order to avoid these problems, we deal with a re-normalized version of the matrix $\hat{U}[I(t), \delta I, \delta t]$, as given in the second line of equation (12); it should be noted here that normalization of the matrix \hat{U}_{Total} is irrelevant for purposes of extracting the measurement basis and fidelity. It is now straightforward to see that an unnormalized version of the matrix \hat{U}_{Total} obeys the equation

$$\frac{d\hat{U}_{\text{Total}}}{dt} = \left(\left[\frac{\langle \hat{\sigma}_n \rangle}{2\tau_m} + \frac{\xi(t)}{2\sqrt{\tau_m}} \right] \hat{\sigma}_n - i\hat{H}_q \hat{\sigma}_z \right) \hat{U}_{\text{Total}}.\tag{24}$$

This equation supplements the stochastic master equation for purposes of interpreting the QPC's output signal in terms of a measurement result. In this context, one should note that what equation (22) gives is the qubit's density matrix as a function of time. When $\beta \neq 0$ and the charge states mix during the measurement, the density matrix at later times can become completely different from that at the start of the measurement process. Assuming that the experimenter does not have any information about the qubit's state at $t = 0$, he would be able to use equation (22) to determine the qubit's state at later times, but he would not be able to cast the results in terms of information that he has learned about the qubit's state at $t = 0$. The matrix \hat{U}_{Total} , through the decomposition explained in section 3.2, contains the information needed to make such a statement about the measurement result. In fact, one can say that, when taken in combination with the initial qubit density matrix, equation (24) replaces equation (22): in addition to containing the measurement information, the matrix \hat{U}_{Total} can be used to calculate the density matrix at any time.

4. Numerical results and discussion

We now present the results of our numerical calculations. Typical parameters of the numerical calculations are as follows: the discrete steps are taken to be $\delta t = 0.1\pi/E$, such that one period of the Hamiltonian-induced coherent oscillations would be divided into 20 steps. The QPC current probability distributions are discretized into 100 possible current values: each distribution is Gaussian with a standard deviation σ of 10 steps (thus there are about 50 possible values for the QPC current with non-negligible occurrence probability). The distance between the two center points of the current probability distributions $\Delta \bar{I}$ determines the qubit-QPC coupling strength. This parameter is varied when analyzing the effect of the qubit-QPC coupling strength on the behavior of the system. The number of time steps in a single calculation was

different for different calculations. However, this number was always large enough that the final qubit state reached perfect purity up to less than one part in 10^5 , ensuring that none of our numerical results were sensitive to the exact choice of this parameter. Each measurement procedure is repeated up to 10^4 times in order to obtain accurate statistical averages. We have also used parameters different from the typical ones given above and found that the results are unaffected by the specific choice of these parameters.

A convenient parameter for purposes of characterizing the qubit–QPC coupling strength is $E\tau_m/(2\pi)$, where τ_m is the timescale needed to obtain sufficient QPC signal to read out the state of the qubit (for the time being one can think of this definition as applying to the case when $\beta = 0$; but see below). As the standard deviation of the QPC-output effective probability distribution scales as σ/\sqrt{N} when the measurement step is repeated N times, the measurement time τ_m can be naturally defined as the product of the time step δt and the value of N at which $2\sigma/\sqrt{N} = \Delta I$. τ_m is therefore given by

$$\tau_m = \frac{4\sigma^2\delta t}{\Delta I^2}. \quad (25)$$

We shall use the parameter $E\tau_m/(2\pi)$ for quantifying the qubit–QPC coupling strength, and we shall use τ_m as a characteristic measurement timescale when presenting our results below.

4.1. Stochastically determined measurement basis

Firstly, in figure 2, we show the spherical coordinates θ and ϕ of a large number of (stochastically determined) measurement bases for different qubit–detector coupling strengths and different values of β . In the strong-coupling regime (top row in figure 2), the parameter $E\tau_m/(2\pi)$ is much smaller than one, and the measurement is completed before any Hamiltonian-induced dynamics can occur. As a result, the measurement basis is always the charge basis, i.e. the natural measurement basis for the detector under consideration (note here that the charge basis is characterized by the direction $(\theta, \phi) = (\beta, 0)$). As the qubit–detector coupling strength is reduced (middle row in figure 2), the measurement bases start to deviate from the charge basis, and they develop some statistical spread. This region could be called the intermediate-coupling regime. Deep in the weak-coupling regime (bottom row in figure 2), the measurement bases are spread over all the possible directions. The probability distribution of possible measurement bases will be analyzed in section 4.4.

When $\beta = 0$ (leftmost column in figure 2), the measurement basis is always the charge basis, regardless of the qubit–QPC coupling strength. This result is natural, since this case is the simple one with no mixing between the states $|L\rangle$ and $|R\rangle$. When $\beta = \pi/2$, all the possible measurement bases lie in the x – y -plane. The reason behind this result lies in the fact that this situation is equivalent to one where one makes a large number of weak measurements in the x – y -plane with no Hamiltonian-induced precession. As explained in appendix C, the resulting measurement bases can only be in the same plane as the actually performed measurements, which is the x – y -plane in this case.

The fact that the measurement basis is generally unpredictable, and therefore uncontrollable, is a rather strange phenomenon from a fundamental point of view. From a practical point of view, one can wonder whether anything useful can be done with such measurements that are performed in a stochastically determined basis. If one absolutely requires

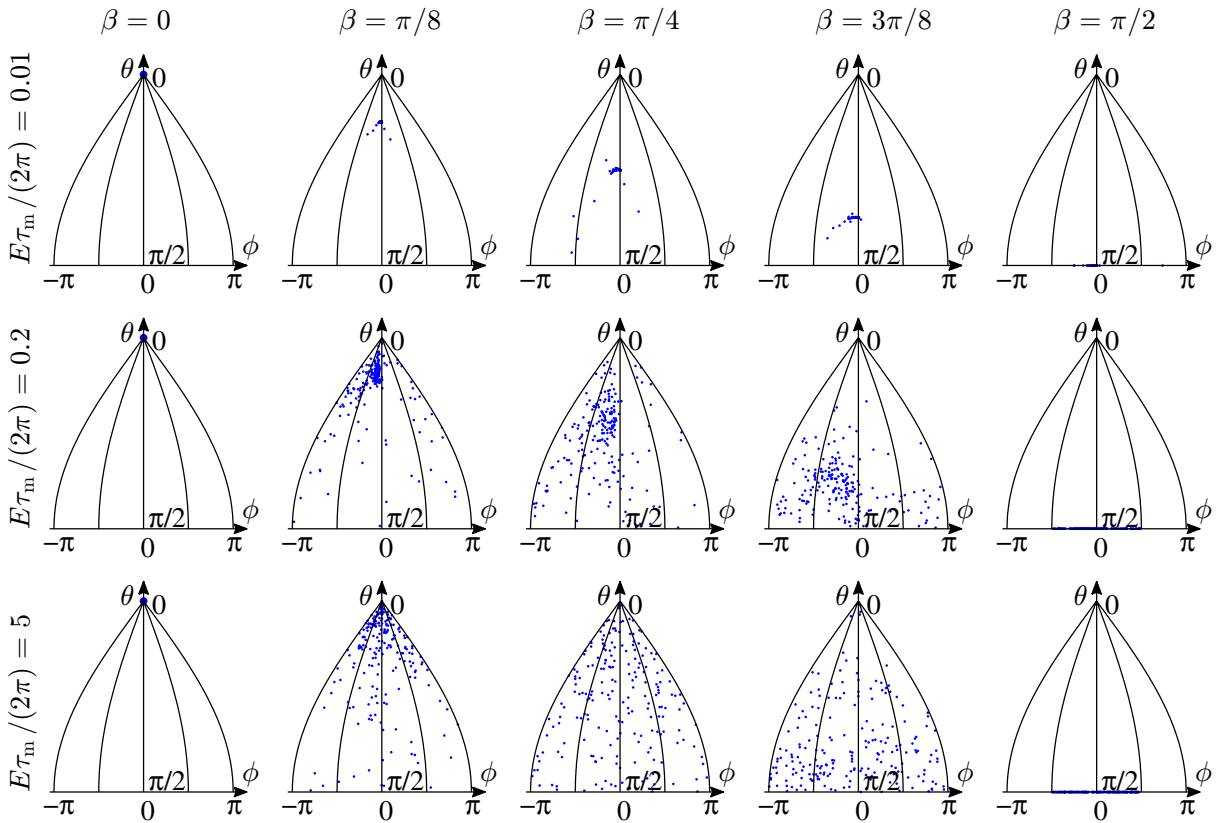


Figure 2. The spherical coordinates θ and ϕ defining the stochastically determined measurement bases obtained in simulations of the experiment under consideration (note that since the measurement basis is defined by an axis extending in two opposite directions, only the upper hemisphere is needed; any measurement axis will either lie in the plane of the equator or have one end above the equator). Each figure contains 200 points. In each row, the qubit–QPC coupling strength is kept fixed and β is varied: $\beta = 0, \pi/8, \pi/4, 3\pi/8$ and $\pi/2$. In each column β is kept fixed and the qubit–QPC coupling strength is varied. In the top row, $E\tau_m/(2\pi) = 0.01$, which is deep in the strong-coupling regime. The measurement basis is very close to the charge basis in about 99% of the runs. In the middle row, $E\tau_m/(2\pi) = 0.2$, which can be identified as the intermediate-coupling regime. The measurement basis deviates substantially from the charge basis in about one-half of the runs. In the bottom row $E\tau_m/(2\pi) = 5$, which is in the weak-coupling regime. The measurement bases are, in general, spread over the entire hemisphere. In generating this figure, the initial state was taken to be the maximally mixed state (note that the results are independent of the initial state).

a measurement in a given basis, measurement results in different bases would be less useful. One could then treat the deviation of the observed measurement basis from the desired one as an experimental error and deal with it accordingly. This point will be discussed further in section 4.5.

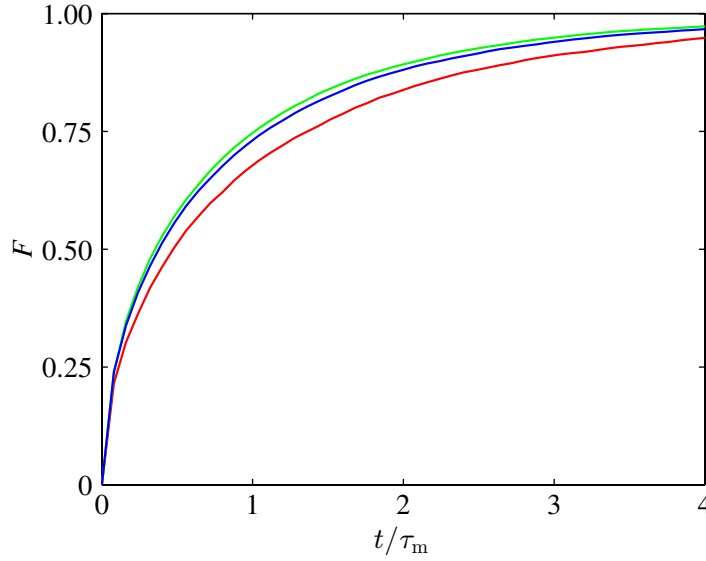


Figure 3. The measurement fidelity as a function of measurement duration for three different values of the angle β between the charge basis and the energy eigenbasis: $\beta = 0$ (red; lowest line), $\pi/4$ (green) and $\pi/2$ (blue). Here $E\tau_m/(2\pi) = 5$, i.e. deep in the weak-coupling regime. The fidelity increases from zero to one as the measurement duration increases, and it is almost independent of the angle β .

4.2. Information acquisition rate

In figure 3, we plot the measurement fidelity as a function of measurement duration for three different values of β (i.e. the angle between the charge basis and the qubit's energy eigenbasis), keeping all other parameters fixed. We can see that the fidelity approaches one for long enough measurement time, regardless of the value of the angle β . Furthermore, the fidelity is almost independent of β . In fact, and rather counter-intuitively, it turns out that the fidelity for $\beta \neq 0$ is higher than that for $\beta = 0$. The reason behind this phenomenon is that one can obtain a higher fidelity by performing weak measurements along different axes rather than along the same axis, as explained in appendix C. This result shows that even though more complicated analysis is needed to extract useful measurement information when $\beta \neq 0$, the information acquisition rate is not reduced, and is in fact enhanced, by the Hamiltonian-induced precession.

In the limit when the fidelity reaches one, the matrix $\hat{U}_{\text{Meas}}[I(t : 0 \rightarrow t_f), \delta I, \delta t]$ has the form $|\psi_1\rangle\langle\psi_1|$. It is straightforward to verify that any further evolution of the system will not affect $\hat{U}_{\text{Meas}}[I(t : 0 \rightarrow t_f), \delta I, \delta t]$. In this case, further measurement only changes the final state of the qubit, which would be given by $\hat{U}_{\text{Rot}}[I(t : 0 \rightarrow t_f), \delta I, \delta t]|\psi_1\rangle$.

It is worth mentioning here that the fidelity for the case $\beta = 0$ is very well fitted by the function

$$F(t) = \text{erf} \left\{ \sqrt{\frac{t}{2\tau_m}} \right\}, \quad (26)$$

where erf stands for the error function. This result can be obtained using the following calculation. We take the probability distribution in equation (A.2) and we replace δt by t . We now

identify the portion of this distribution that corresponds to $I > (\bar{I}_L + \bar{I}_R)/2$ as being the probability of making a wrong inference about the state of the qubit. The difference between the probability of making a correct inference about the state of the qubit and that of making a wrong inference gives equation (26). The fidelity in figure 3 is also relatively well fitted by the function

$$F(t) \approx 1 - \exp\left\{-\frac{t}{\tau_m}\right\}, \quad (27)$$

which is an indication that our definition for the measurement time τ_m (see appendix A) is a reasonable one.

4.3. The information contained in the QPC's output signal

The QPC produces an output signal that contains fast and large fluctuations. There are therefore a very large number of possible output signals that the QPC can display. We now ask the question of what information is contained in a given QPC output signal. It turns out that only a small amount of information in the signal concerns the state of the qubit. As explained above, one can follow a conceptually straightforward calculation in order to extract the measurement basis, measurement result and fidelity from the noisy signal. The signal also contains information about how the qubit's state is rotated after the effective measurement. It should be noted here that measurement bases and post-measurement rotations generally come in all possible combinations. The measurement basis, result and fidelity on the one hand and the post-measurement rotation on the other hand can therefore be seen as two separate pieces of information that are contained in the QPC's output signal. The rest of the information contained in the highly noisy signal, which is the vast majority of information contained in the signal, concerns the QPC itself. Thus the large fluctuations that one observes provide information about the state of the QPC in the specific experimental run under consideration. For purposes of reading out the state of the qubit, this information is discarded. This situation is most clearly demonstrated in the case $\beta = 0$, where one is only interested in the time average of the signal, discarding all the fluctuations around the average.

4.4. Spectral analysis of the measurement-basis probability distribution

We now take sets of stochastically determined measurement bases (i.e. results of the kind presented in figure 2) and use them to extract probability distributions $g(\theta, \phi)$ for the measurement basis. The probability distributions are normalized to unity: $\int g(\theta, \phi) d\Omega = 1$ with the integral covering the hemisphere $0 \leq \theta \leq \pi/2$, $0 \leq \phi \leq 2\pi$. In particular, we are interested in these probability distributions in the weak-coupling regime. In this regime, the probability distributions will be symmetric about the z -axis, i.e. $g(\theta, \phi)$ will be independent of ϕ . We use this fact and write the probability distribution as

$$g(\theta, \phi) = \sum_{n=0}^{\infty} c_n Y_{n,0}(\theta, \phi), \quad (28)$$

where $Y_{n,0}(\theta, \phi)$ are the usual spherical harmonics given by

$$Y_{n,0}(\theta, \phi) = \sqrt{\frac{2n+1}{4\pi}} P_n(\cos \theta), \quad (29)$$

and $P_n(x)$ are the Legendre polynomials. Note that since we only need to consider the hemisphere $0 \leq \theta \leq \pi/2$, we only need to keep even values of n in the above series. The coefficients c_n are given by

$$c_n = 2 \int_0^{\pi/2} d\theta \sin \theta \int_0^{2\pi} d\phi g(\theta, \phi) Y_{n,0}(\theta, \phi). \quad (30)$$

In our calculations, we have a collection of N stochastically determined measurement bases. The coefficients c_n can be calculated from these data sets using the formula

$$c_n = \frac{2}{N} \sum_j Y_{n,0}(\theta_j, \phi_j), \quad (31)$$

where the index j labels the different data points.

In order to ensure that we are using parameters that are sufficiently deep in the weak-coupling regime, we start by performing the above spectrum analysis while varying $E\tau_m/(2\pi)$. The results of this calculation for $\beta = \pi/8$ are shown in figure 4(a). The coefficients c_n seem to be almost independent of $E\tau_m/(2\pi)$ when this parameter is larger than one. From these results we conclude that the point $E\tau_m/(2\pi) = 5$ is sufficiently deep in the weak-coupling regime for purposes of calculating $g(\theta, \phi)$ in the limit $E\tau_m/(2\pi) \rightarrow \infty$.

We now calculate c_n (up to $n = 10$) in the weak-coupling regime for different values of β and plot the results in figure 4(b). The probability distribution changes gradually as we go from $\beta = 0$, where the measurement basis is always along the z -axis (here the charge basis), to $\beta = \pi/2$, where the measurement basis is always in the x - y -plane. There is one point ($\beta \approx 0.3\pi$) where $g(\theta, \phi)$ is either approximately or exactly uniform over the entire hemisphere.

4.5. Short-time dynamics

We now consider the case where the measurement duration is short enough that the measurement fidelity is much smaller than one. In this case the state of the qubit experiences only a small amount of projective evolution. As a result we can calculate analytically the total effect of the projection and coherent dynamics.

Dividing the total time interval under consideration into a large number of infinitesimal intervals, we can write the total evolution matrix as

$$\begin{aligned} \hat{U}_{\text{Total}} [I(t : 0 \rightarrow t_f), \delta I, \delta t] &\approx [1 + \delta p(t_f) \hat{\sigma}_n] e^{i\hat{\sigma}_z E \delta t/2} \dots e^{i\hat{\sigma}_z E \delta t/2} [1 + \delta p(\delta t) \hat{\sigma}_n] e^{i\hat{\sigma}_z E \delta t/2} [1 + \delta p(0) \hat{\sigma}_n] \\ &= e^{i\hat{\sigma}_z E t_f/2} [1 + \delta p(t_f) \hat{\sigma}_n(t_f)] \times \dots \times [1 + \delta p(\delta t) \hat{\sigma}_n(\delta t)] \times [1 + \delta p(0) \hat{\sigma}_n(0)] \\ &\approx e^{i\hat{\sigma}_z E t_f/2} [1 + \delta p(t_f) \{ \sin \beta \cos(E t_f) \hat{\sigma}_x + \sin \beta \sin(E t_f) \hat{\sigma}_y + \cos \beta \hat{\sigma}_z \}] \times \dots \\ &\quad \times [1 + \delta p(0) \{ \sin \beta \cos(0) \hat{\sigma}_x + \sin \beta \sin(0) \hat{\sigma}_y + \cos \beta \hat{\sigma}_z \}] \\ &\approx e^{i\hat{\sigma}_z E t_f/2} \left[1 + \int_0^{t_f} dt \frac{\delta p(t)}{\delta t} \{ \sin \beta \cos(E t) \hat{\sigma}_x + \sin \beta \sin(E t) \hat{\sigma}_y + \cos \beta \hat{\sigma}_z \} \right] \\ &= e^{i\hat{\sigma}_z E t_f/2} [1 + p_x \hat{\sigma}_x + p_y \hat{\sigma}_y + p_z \hat{\sigma}_z], \end{aligned} \quad (32)$$

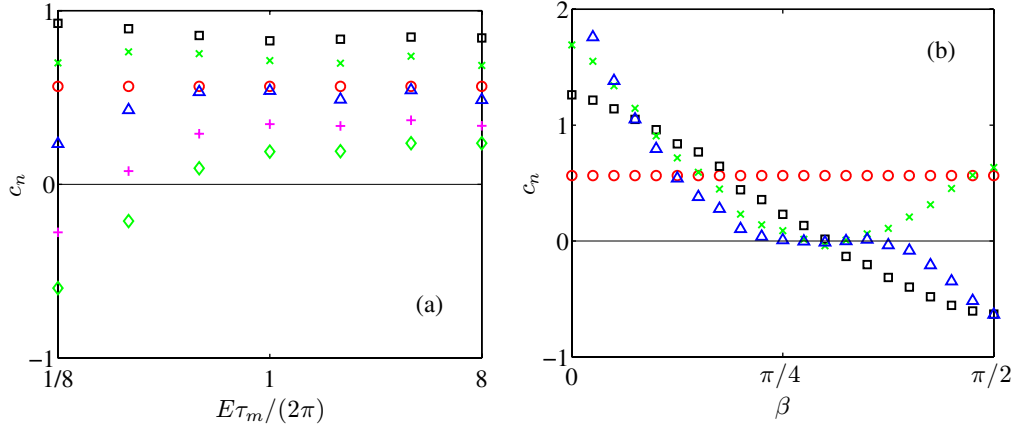


Figure 4. Spectral analysis of the probability distribution $g(\theta, \phi)$: (a) the spectral components c_n for $n = 0$ (red circles), 2 (black squares), 4 (green \times symbols), 6 (blue triangles), 8 (purple + signs) and 10 (green diamonds) as functions of $E\tau_m/(2\pi)$ for $\beta = \pi/8$. Note the logarithmic scale on the x -axis. As $E\tau_m/(2\pi)$ is increased, the spectral components clearly reach very stable values by the time $E\tau_m/(2\pi)$ reaches one. These results indicate that the value $E\tau_m/(2\pi) = 5$ is sufficiently deep in the weak-coupling regime for purposes of studying the limit $E\tau_m/(2\pi) \rightarrow \infty$. (b) The spectral components c_n for $n = 0, 2, 4$ and 6 (same symbol usage as in (a)) as functions of β in the weak-coupling regime (here we use the value $E\tau_m/(2\pi) = 5$). As β is increased, the probability distribution $g(\theta, \phi)$ gradually changes from being concentrated at the energy eigenbasis to being spread over all directions and then to being concentrated on the equator perpendicular to the energy eigenbasis. There seems to be one value of β (close to 0.3π , which is close to $\cos^{-1}(1/\sqrt{3})$) where all the spectral components with $n \neq 0$ vanish, i.e. $g(\theta, \phi)$ becomes completely uniform.

where we have defined

$$\begin{aligned} \delta p(t) &= \frac{\delta t [I(t) - \bar{I}]}{\tau_m \Delta \bar{I}}, \\ \mathbf{n}(t) &= \sin \beta \cos(Et) \hat{x} + \sin \beta \sin(Et) \hat{y} + \cos \beta \hat{z}, \\ p_x &= \sin \beta \int_0^{t_f} \frac{I(t) - \bar{I}}{\tau_m \Delta \bar{I}} \cos(Et) dt, \\ p_y &= \sin \beta \int_0^{t_f} \frac{I(t) - \bar{I}}{\tau_m \Delta \bar{I}} \sin(Et) dt, \\ p_z &= \cos \beta \int_0^{t_f} \frac{I(t) - \bar{I}}{\tau_m \Delta \bar{I}} dt. \end{aligned} \quad (33)$$

Taking the total measurement duration t_f to be a multiple of the qubit's free-precession period, the different measurements strengths $p_{x,y,z}$ are different Fourier components of the observed QPC signal. These Fourier components can be thought of as independent quantities, leading one to think of the net result as three independent weak measurements, one along each of the three axes x , y and z .

We have performed spectral analysis as was done in section 4.4 on the possible measurement outcomes in the short-time case analyzed above (we do not show the full results here). In the calculations, p_x , p_y and p_z were assumed to be Gaussian-distributed quantities with root-mean-square values that obey the relation

$$p_x^{\text{rms}} : p_y^{\text{rms}} : p_z^{\text{rms}} = \frac{\sin \beta}{\sqrt{2}} : \frac{\sin \beta}{\sqrt{2}} : \cos \beta. \quad (34)$$

The overall features of the dependence of c_n on β are similar to those seen in figure 4(b), but there is no exact agreement between the two cases. For example, the coefficient c_2 is close to being a straight line all the way from $\beta = 0$ to $\beta = \pi/2$ in the present case, as opposed to the curved path that the black squares follow in figure 4(b). Finally, we ask whether there is a value of β at which all three measurements have the same strength on average. Using equation (34) it is straightforward to see that this situation occurs when $\cos \beta = 1/\sqrt{3}$, i.e. $\beta = 0.304\pi$; the point at which all measurement directions are equally probable in figure 4(b). The calculations of this subsection therefore give us a simple interpretation of the significance of the point $\beta = 0.3\pi$ in the present context.

4.6. Alternative interpretation: choosing the measurement basis independently of the measurement outcome

The idea that the measurement basis is determined stochastically and is only specified when the experiment is completed is conceptually unsettling. We therefore take a different approach in this section. We now require that in order to have a meaningful measurement, the measurement basis must be specified by the setup and not by the stochastically determined measurement outcome.

In the strong-coupling regime, there are no conceptual problems. In this case, the measurement is almost instantaneous, and the measurement basis is clearly the charge basis. The measurement fidelity is almost 100%, up to errors caused by the finiteness of the measurement time compared to the qubit-precession period. These errors can be quantified straightforwardly, as we shall do shortly.

The weak-coupling regime is the one where the conceptual problems arise. If we take the case where the distribution of measurement bases is essentially uniform over all direction (which seems to be the case when $\beta \approx 0.3\pi$), we again obtain a simple, yet somewhat surprising, result. By symmetry we can argue that all directions are equivalent. We can therefore choose any basis as the measurement basis. Based on this choice, we then divide all the different possible outcomes (i.e. the different possible QPC output signals) into two sets, one of which corresponds to the measurement result +1 and the other of which corresponds to the result -1 in the chosen basis. An important question that arises in this scenario is what the average measurement fidelity would be under such ‘worst-case’ conditions of having no preferred measurement basis. In the following, we shall denote this average measurement fidelity by the symbol \bar{F} in order to stress the difference between the results of this subsection and those of section 4.2. For the completely uniform case, the average fidelity \bar{F} can be evaluated as follows: let us take a spin pointing in the +z-direction and assume that we have specified the z-axis as the one defining the measurement basis. If we measure the spin along an axis that makes an angle θ with the z-axis, we obtain the result +1 with probability $\cos^2(\theta/2)$ and the result -1 with probability $\sin^2(\theta/2)$. By dividing the possible outcomes into two sets (with all outcomes that correspond to states in the upper hemisphere being interpreted as +1 along the z-axis and all outcomes that

correspond to states in the lower hemisphere being interpreted as -1 along the z -axis) and taking the difference between the probability of correctly obtaining the result $+1$ and the probability of obtaining the wrong result -1 , we find that the average fidelity (averaged uniformly over the entire hemisphere)

$$\bar{F}_{\text{uniform}, E\tau_m \rightarrow \infty} = \int_0^{\pi/2} d\theta \sin \theta \left(\cos^2 \frac{\theta}{2} - \sin^2 \frac{\theta}{2} \right) = \frac{1}{2}. \quad (35)$$

The fidelity in this ‘worst-case scenario’ is therefore 50%. We emphasize again that this fidelity is independent of our choice of measurement basis. This result again contrasts the usual intuition where the outcomes of measurements performed in one basis provide no information at all in an orthogonal basis. In the present case, all measurement bases are equivalent, and one would obtain the same (average) measurement fidelity in any one of them. This result fits well with the result that will be explained in section 4.7 that quantum state tomography can be performed by repeating the same measurement procedure a large number of times. This measurement procedure gives the same amount of information in all different bases.

As explained above, the lowest possible average fidelity is 50%, and it occurs when $\beta \approx 0.3\pi$. Two other values of β allow for simple reasoning. The obvious one is the case of $\beta = 0$, where the measurement basis is $\{|L\rangle, |R\rangle\}$ and the fidelity is 100% for all coupling strengths. The other exception occurs when $\beta = \pi/2$. As can be seen from the rightmost column of figure 2, the measurement basis is always in the x - y -plane. In the weak-coupling regime, the possible measurement bases are spread uniformly around the equator. In that limit, one can choose any axis in the x - y -plane as defining the measurement basis. All these bases give the same value for the average fidelity:

$$\bar{F}_{\beta=\pi/2, E\tau_m \rightarrow \infty} = \frac{1}{2\pi} \int_0^{2\pi} d\phi \left| \cos^2 \frac{\theta}{2} - \sin^2 \frac{\theta}{2} \right| = \frac{2}{\pi}. \quad (36)$$

Numerical results for the average fidelity for different values of β in the weak-coupling limit are plotted in figure 5. First, in figure 5(a), we plot the average fidelity as a function of the chosen measurement angle θ_{Meas} for different values of β . We find that for $\beta < 0.3\pi$ choosing the energy eigenbasis as the measurement basis gives the highest average fidelity, whereas for $\beta > 0.3\pi$ choosing a basis that is orthogonal to the energy eigenbasis gives the highest average fidelity (note that there is an infinite number of such bases). In figure 5(b), we plot the average fidelity as a function of β for three choices of the measurement basis: $\theta_{\text{Meas}} = 0$, $\theta_{\text{Meas}} = \pi/2$ and the charge basis. It should be noted here that in the weak-coupling limit there is symmetry about the z -axis. As a result, any axis that is obtained by rotating the charge basis about the Hamiltonian axis will result in the same value of the fidelity as the charge basis. Choosing the charge basis as the measurement basis never results in an average fidelity that is substantially lower than the maximum possible value.

In the intermediate-coupling regime, one can choose the measurement basis by maximizing the average fidelity. For example, for the parameters of the middle row in figure 2 one can see that the measurement basis that would maximize the fidelity deviates slightly from the charge basis (unless $\beta = 0$). One can understand this result naturally by keeping in mind that the qubit’s state precesses about the Hamiltonian’s axis while being measured. The measurement basis is therefore approximately obtained by taking the charge basis and rotating it by the appropriate angle about the qubit Hamiltonian (in the opposite sense from state precession).

One could perform a numerical calculation in order to analyze the behavior of the maximum-fidelity measurement basis as the qubit–detector coupling strength is varied.

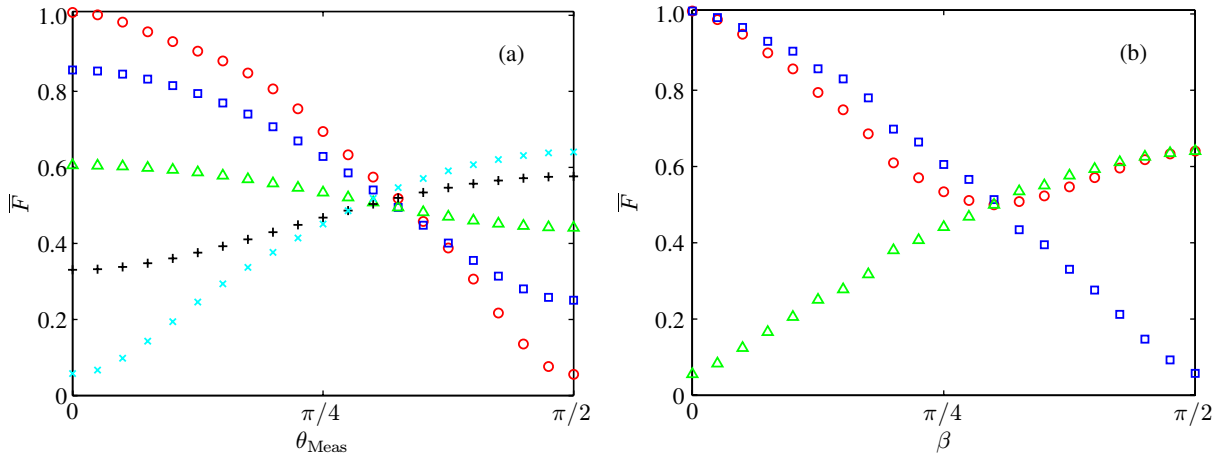


Figure 5. The average fidelity \bar{F} when defining the measurement basis independently of the specific (stochastic) outcome in the weak-coupling regime [$E\tau_m/(2\pi) = 5$]: (a) the average fidelity as a function of the ‘manually’ chosen measurement angle θ_{Meas} for five different values of β : 0 (red circles), $\pi/8$ (blue squares), $\pi/4$ (green triangles), $3\pi/8$ (black + signs) and $\pi/2$ (cyan \times symbols). Note that the results are independent of the choice of the azimuthal angle ϕ_{Meas} , which is also chosen manually along with θ_{Meas} . One can see that for any value of β the maximum fidelity is obtained by choosing either $\theta_{\text{Meas}} = 0$ (for $\beta < 0.3\pi$) or $\theta_{\text{Meas}} = \pi/2$ (for $\beta > 0.3\pi$). For $\beta = 0.3$ (not shown) all values of θ_{Meas} give essentially the same value for the fidelity, namely 50%. (b) The average fidelity as a function of β for three different choices of measurement angle θ_{Meas} : $\theta_{\text{Meas}} = 0$ (blue squares), $\theta_{\text{Meas}} = \beta$ (red circles) and $\theta_{\text{Meas}} = \pi/2$ (green triangles). The choice $\theta_{\text{Meas}} = \beta$ always gives a near or true maximum in the fidelity. However, with the exception of a single point around $\beta = 0.3\pi$, the maximum occurs at either $\theta_{\text{Meas}} = 0$ or $\theta_{\text{Meas}} = \pi/2$.

However, here we focus on a question that seems more experimentally relevant, namely analyzing the measurement fidelity with the charge basis chosen as the measurement basis. This fidelity is shown in figure 6 for the two cases $\beta = \pi/4$ and $\beta = \pi/2$. In figure 7, we plot the absolute value of the quantity $2\pi d\bar{F}/d(E\tau_m)$ (i.e. as in the initial slope in figure 6) as a function of β . This quantity can be used to obtain an estimate for the measurement errors associated with having a finite measurement time.

4.7. Small-current case

In the above analysis, we have assumed that the QPC’s output is essentially a continuous variable with a large number of possible values for the current at a given instant. If the QPC’s current is so small that on the timescale of monitoring the output signal very few electrons can tunnel through the QPC, the physical picture changes substantially (here we assume that the number of electrons that have tunneled through the QPC can be measured accurately). One now has a small number of possible values for the QPC’s output signal. The discretization used in our analysis, which was done for computational convenience above, is now provided naturally by

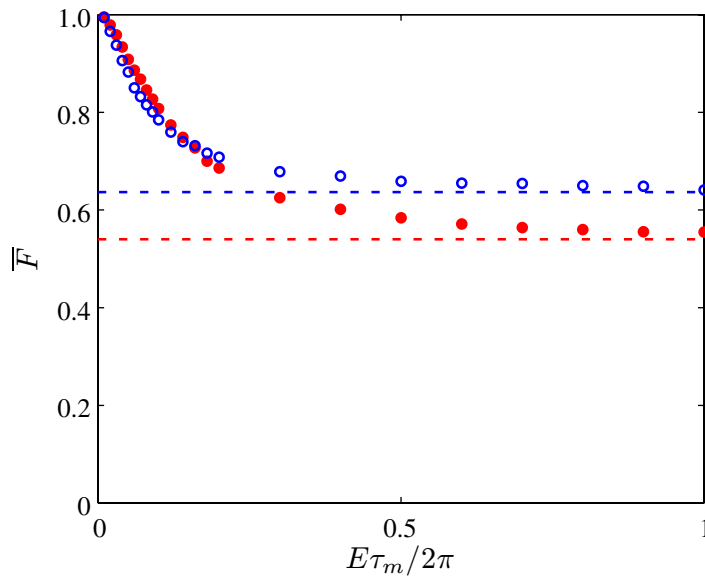


Figure 6. The average fidelity \bar{F} as a function of $E\tau_m/(2\pi)$ when the measurement basis is decided (by the experimenter) to be the charge basis. The blue open circles correspond to the case $\beta = \pi/4$, and the red filled circles correspond to the case $\beta = \pi/2$. The dashed lines represent the asymptotic values of the fidelity in the weak-coupling limit: 0.54 for the case $\beta = \pi/4$ and $2/\pi$ for the case $\beta = \pi/2$.

the design of the setup. One can then follow a similar analysis to that of section 3 concerning the gradual progression of the measurement and the evolution of the quantum state of the qubit. Note that considering the small-current case only makes sense if the number of electrons that tunnel through the QPC during a full qubit-precession period is small. Otherwise, one can always choose between the small- and large-current cases through the choice of δt . Clearly, the exact choice of parameters used in the theoretical analysis cannot affect the physical results.

An important difference between the cases of small and large currents is that one expects the probability distributions shown in figure 1(b) to have almost symmetric shapes for the large-current case, whereas they almost certainly are not symmetric for the small-current case. This point is most clearly seen by considering the situation where at most one electron tunnels through the QPC during the short interval under consideration. The analysis and results in this case follow closely the analysis and results for a switching-based detector, studied recently in [18]. The fact that, unlike the case of a switching-based detector, the measurement now continues after the occurrence of a tunneling event can be incorporated into the analysis straightforwardly. Our argument concluding that the choice of the measurement basis is independent of the initial state of the qubit breaks down. Perhaps more importantly, the conceptual picture that the measurement basis is chosen first (according to some probability distribution) and the measurement result is then obtained in that basis becomes invalid. For example, it is now possible for a certain state $|\psi\rangle$ to be a possible result of the data analysis presented above, but not the state orthogonal to it [18].

It is also worth mentioning in this context the case where the tunneling process is coherent on the timescale of qubit precession. In this case, the QPC measures the qubit in the energy

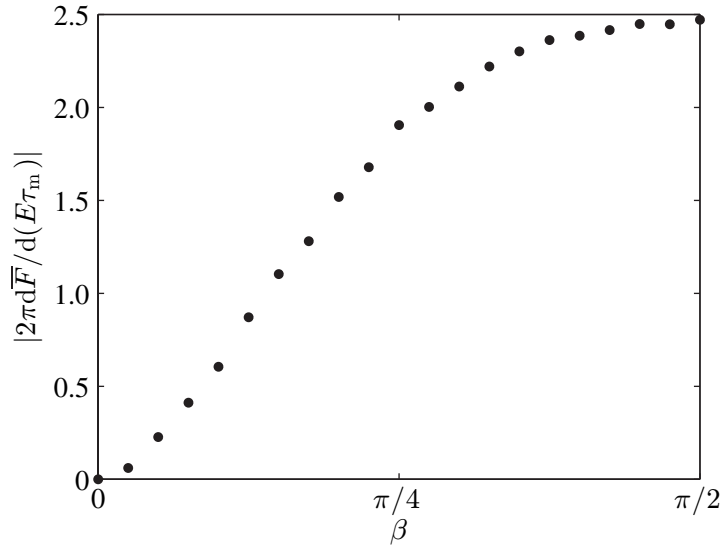


Figure 7. The rate of charge-basis fidelity deterioration with increasing measurement time $|2\pi d\bar{F}/d(E\tau_m)|$ as a function of β in the strong-coupling regime. In other words, the quantity on the y-axis is the absolute value of the slope of curves similar to those shown in figure 6 at $E\tau_m/2\pi = 0$. Each data point is determined by calculating the fidelity \bar{F} at $E\tau_m/(2\pi) = 0.06$ for a given value of β and then taking the ratio $[1 - \bar{F}(x)]/x$, where $x = E\tau_m/(2\pi)$.

eigenbasis, regardless of the angle β (except when $\beta = \pi/2$ where the QPC fails to perform any measurement on the qubit). For further discussion of this case, see e.g. [5], and for a discussion of possible advantages of weak measurement when dealing with multi-qubit circuits, see e.g. [19].

4.8. Quantum state tomography

One example of a procedure where the uncontrollability of the measurement basis can be harmless is quantum state tomography (QST). In fact, the original idea of QST included performing measurements in all possible bases [20]. We have simulated QST by repeating the measurement procedure a large number of times, obtaining a set of measurement results (in the form of pre-measurement qubit states), and then minimizing the function (see appendix D)

$$\mathcal{T}(r, \theta, \phi) = \sum_j [1 - r \cos \Omega(\theta, \phi, \theta_j, \phi_j)]^2, \quad (37)$$

where r , θ and ϕ are the spherical coordinates of a point in the Bloch sphere; j is an index labeling the different runs of the experiment, the direction (θ_j, ϕ_j) defines the qubit state obtained in a given measurement, and $\Omega(\theta, \phi, \theta_j, \phi_j)$ is the angle between the directions (θ, ϕ) and (θ_j, ϕ_j) . We have chosen several initial states covering the Bloch sphere, and the tomography procedure always produced correctly the initial state of the qubit. For the largest value of the qubit–detector coupling strength that we used (see top row of figure 2), the procedure became unreliable, because the vast majority of the measurements are performed in one basis.

It is worth pausing here to ask the question of the minimum requirements for a single measurement setting to provide full QST information. The qubit's density matrix is characterized by three parameters. One therefore needs the ensemble of measurements to produce three independent variables. If the detector has four possible outcomes (or output signals), one would obtain three independent probabilities for three of the outcomes (with the probability of obtaining the fourth outcome determined by probability normalization). A four-outcome detector is therefore sufficient, in principle, to perform full QST on a qubit. One can generalize this argument straightforwardly to the case of larger systems: one needs a detector with at least as many possible outcomes as the square of the size of the Hilbert space in order to perform QST in that Hilbert space (we do not necessarily imply pure states here).

In [18] an 'all-in-one' measurement procedure was analyzed, where the measurement results of identically prepared setups (using a switching-based detector) can be used to perform full state tomography of the initial qubit state as well as extract all relevant system parameters. One could ask whether a similar situation occurs in the qubit-QPC system. The answer is yes, in principle. However, because the analysis of [18] was almost entirely analytic, it was possible to obtain simple expressions to which the measurement data would be fitted in order to extract all the available parameters. In this paper, we have not been able to obtain similar analytic expressions. As a result, it would require extensive numerical calculations to compare the observed data with those that would be expected for all possible sets of parameters and then find the parameters that produce the best fit. Given the relatively long computation times required for even the simple numerical calculations presented in this paper, we have not attempted to simulate the full parameter-extraction procedure.

5. Decoherence

So far we have assumed that there is no decoherence in the system other than that associated with the measurement-induced projection. In this section, we briefly consider the effect of additional decoherence channels on the measurement process.

As a first step, one can make the following observations: the measurement has a characteristic time τ_m , which determines how long it takes for the experimenter to obtain a high-fidelity measurement result. Decoherence introduces its own decoherence timescales, which we collectively denote by τ_d . If $\tau_m \ll \tau_d$, decoherence should have little effect on the analysis and results of the previous sections. If, on the other hand, $\tau_m \gg \tau_d$, decoherence will distort the state of the qubit before any reliable measurement result is obtained. This situation renders the measurement almost completely useless. One should keep in mind, however, that the above statement depends strongly on the nature of the decoherence channel. For example, if the energy eigenbasis coincides with the charge basis (i.e. there is no coherent dynamics mixing the states $|L\rangle$ and $|R\rangle$) and there is no relaxation between the states $|L\rangle$ and $|R\rangle$, pure dephasing between these states will not hamper the measurement, regardless of the dephasing time.

Decoherence can also be introduced to the stochastic master equation such that equation (22) turns into:

$$\begin{aligned} \dot{\rho}_q = & -i \left[\hat{H}_q, \rho_q \right] + \frac{\xi(t)}{2\sqrt{\tau_m}} \left(\hat{\sigma}_n \rho_q + \rho_q \hat{\sigma}_n - 2 \langle \hat{\sigma}_n \rangle \rho_q \right) + \frac{1}{4\tau_m} \left(\hat{\sigma}_n \rho_q \hat{\sigma}_n - \rho_q \right) \\ & + \sum_k \gamma_k \left(\hat{A}_k \rho_q \hat{A}_k^\dagger - \frac{1}{2} \hat{A}_k^\dagger \hat{A}_k \rho_q - \frac{1}{2} \rho_q \hat{A}_k^\dagger \hat{A}_k \right), \end{aligned} \quad (38)$$

where the index k represents the different decoherence channels, with γ_k and \hat{A}_k being the rate and quantum operator that describe a given decoherence channel.

Modifying equation (24) in order to include decoherence is somewhat trickier. The difficulty lies in the fact that the evolution of the density matrix is no longer of the form

$$\rho_q \rightarrow \hat{U} \rho_q \hat{U}^\dagger, \quad (39)$$

ignoring here terms in equation (22) that were added for normalization purposes. One way to deal with this new difficulty is to note that the evolution of the density matrix caused by decoherence is linear and therefore write the qubit's density matrix in vector form, i.e. the transpose of $(\rho_{00}, \rho_{11}, \rho_{01}, \rho_{10})$. With this rearrangement of the matrix elements, the evolution matrices are now expressed as 4×4 matrices acting on the density matrix (which now looks like a vector) from the left:

$$\rho_q \rightarrow \hat{\mathcal{U}} \rho_q, \quad (40)$$

where we now use the symbol $\hat{\mathcal{U}}$ in order to distinguish the 4×4 matrices of this section from the 2×2 matrices that are applied symmetrically on both sides of the density matrix.

We shall not write down the detailed expressions for the evolution matrices $\hat{\mathcal{U}}$, because they would not add insight into the present discussion. Instead we point out that deriving a master equation for these matrices can be done straightforwardly by rearranging equation (38) into vector format. The differential equation that describes the evolution of the density matrix ρ_q also describes the evolution of the propagator $\hat{\mathcal{U}}_{\text{Total}}$, similarly to the fact that the Schrödinger equation can be applied to wavefunctions or propagators. We now assume that the total evolution matrix $\hat{\mathcal{U}}_{\text{Total}}$ (including the effects of measurement, Hamiltonian-induced dynamics and decoherence) has been obtained using such a stochastic equation, and we ask the question of how to extract measurement information from it. The answer is a generalized version of the one obtained in the absence of decoherence. The total evolution matrix can be decomposed into two matrices: a measurement matrix followed by a trace-preserving 'quantum operation'. This quantum-operation part describes both unitary evolution and decoherence [22]. The measurement matrix can be used to extract the measurement basis, result and fidelity, just as was done in the absence of decoherence.

We now give a simple example illustrating the interplay between measurement and decoherence. We assume that the Hamiltonian is diagonal in the charge basis, and therefore there is no coherent dynamics between the states $|L\rangle$ and $|R\rangle$. A measurement matrix that corresponds to an outcome that occurs with probability P for the maximally mixed state and has fidelity M now takes the form

$$\hat{\mathcal{U}}_{\text{Meas}}(P, M) = P \begin{pmatrix} 1 \pm M & 0 & 0 & 0 \\ 0 & 1 \mp M & 0 & 0 \\ 0 & 0 & \sqrt{1-M^2} & 0 \\ 0 & 0 & 0 & \sqrt{1-M^2} \end{pmatrix}, \quad (41)$$

A relaxation matrix with relaxation factor D_r (which can be thought of as decaying from one to zero as time goes by) is given by

$$\hat{\mathcal{U}}_{\text{relaxation}}(D_r) = \begin{pmatrix} 1 & 1 - D_r & 0 & 0 \\ 0 & D_r & 0 & 0 \\ 0 & 0 & \sqrt{D_r} & 0 \\ 0 & 0 & 0 & \sqrt{D_r} \end{pmatrix}, \quad (42)$$

and a dephasing matrix with dephasing factor D_p is given by

$$\hat{U}_{\text{dephasing}}(D_p) = \begin{pmatrix} 1 & 0 & 0 & 0 \\ 0 & 1 & 0 & 0 \\ 0 & 0 & D_p & 0 \\ 0 & 0 & 0 & D_p \end{pmatrix}. \quad (43)$$

If a qubit is measured, with the measurement outcome corresponding to the matrix $\hat{U}_{\text{Meas}}(P, M)$, and the qubit then relaxes and dephases according to the matrices $\hat{U}_{\text{relaxation}}(D_r)$ and $\hat{U}_{\text{dephasing}}(D_p)$, the total evolution matrix describing this sequence of events is given by

$$\begin{aligned} \hat{U}_{\text{Total}} &= \hat{U}_{\text{dephasing}}(D_p) \hat{U}_{\text{relaxation}}(D_r) \hat{U}_{\text{Meas}}(P, M) \\ &= P \begin{pmatrix} 1 \pm M & (1 - D_r)(1 \mp M) & 0 & 0 \\ 0 & D_r(1 \mp M) & 0 & 0 \\ 0 & 0 & D_p \sqrt{D_r} \sqrt{1 - M^2} & 0 \\ 0 & 0 & 0 & D_p \sqrt{D_r} \sqrt{1 - M^2} \end{pmatrix}. \end{aligned} \quad (44)$$

This matrix will be used as a reference matrix for the scenario that we describe below. In particular, we shall use the fact that the measurement fidelity is given in terms of the matrix elements in the top left corner:

$$F = \left| \frac{\mathcal{U}_{\text{Total}}^{1,1} - \mathcal{U}_{\text{Total}}^{1,2} - \mathcal{U}_{\text{Total}}^{2,2}}{\mathcal{U}_{\text{Total}}^{1,1} + \mathcal{U}_{\text{Total}}^{1,2} + \mathcal{U}_{\text{Total}}^{2,2}} \right|. \quad (45)$$

We now consider a qubit that is constantly being probed by the QPC while undergoing gradual relaxation and dephasing. The measurement-induced evolution is now expressed as

$$\begin{aligned} \hat{U}_M \rho \hat{U}_M^\dagger &\propto \left[1 + \frac{\delta t [I(t) - \bar{I}]}{\tau_m \Delta \bar{I}} \hat{\sigma}_z \right] \begin{pmatrix} \rho_{00} & \rho_{01} \\ \rho_{10} & \rho_{11} \end{pmatrix} \left[1 + \frac{\delta t [I(t) - \bar{I}]}{\tau_m \Delta \bar{I}} \hat{\sigma}_z \right] \\ &\rightarrow \begin{pmatrix} 1 + G(t) + \frac{\delta t}{4\tau_m} & 0 & 0 & 0 \\ 0 & 1 - G(t) + \frac{\delta t}{4\tau_m} & 0 & 0 \\ 0 & 0 & -\frac{\delta t}{4\tau_m} & 0 \\ 0 & 0 & 0 & -\frac{\delta t}{4\tau_m} \end{pmatrix} \begin{pmatrix} \rho_{00} \\ \rho_{11} \\ \rho_{01} \\ \rho_{10} \end{pmatrix}, \end{aligned} \quad (46)$$

where

$$G(t) = \frac{2\delta t [I(t) - \bar{I}]}{\tau_m \Delta \bar{I}}. \quad (47)$$

Using the above form for the evolution matrix and similar ones for relaxation and dephasing, we arrive at the equation of motion for (an unnormalized version of) the total evolution matrix:

$$\delta \hat{U} = \delta t \begin{pmatrix} G(t) & \gamma_r & 0 & 0 \\ 0 & -\gamma_r - G(t) & 0 & 0 \\ 0 & 0 & -\frac{\gamma_r}{2} - \gamma_p - \frac{1}{2\tau_m} & 0 \\ 0 & 0 & 0 & -\frac{\gamma_r}{2} - \gamma_p - \frac{1}{2\tau_m} \end{pmatrix} \hat{U}, \quad (48)$$

with the initial condition

$$\hat{U}_{\text{Total}}(t=0) = \begin{pmatrix} 1 & 0 & 0 & 0 \\ 0 & 1 & 0 & 0 \\ 0 & 0 & 1 & 0 \\ 0 & 0 & 0 & 1 \end{pmatrix}. \quad (49)$$

The solution of the above differential equation is

$$\hat{U}_{\text{Total}}(t) = \begin{pmatrix} \tilde{G}(0, t) & \gamma_r \int_0^t e^{-\gamma_r t'} \tilde{G}^{-1}(0, t') \tilde{G}(t', t) dt' & 0 & 0 \\ 0 & e^{-\gamma_r t} \tilde{G}^{-1}(0, t) & 0 & 0 \\ 0 & 0 & \exp\left[-\left(\frac{\gamma_c}{2} + \gamma_p + \frac{1}{2\tau_m}\right)t\right] & 0 \\ 0 & 0 & 0 & \exp\left[-\left(\frac{\gamma_c}{2} + \gamma_p + \frac{1}{2\tau_m}\right)t\right] \end{pmatrix}, \quad (50)$$

where

$$\tilde{G}(t_1, t_2) = \exp\left\{\int_{t_1}^{t_2} G(t) dt\right\}. \quad (51)$$

Comparing this matrix with the one in equation (44), one can see that the full dynamics between times 0 and t is equivalent to a measurement that is followed by relaxation and dephasing operations. With some straightforward algebra, one can extract the measurement fidelity:

$$\begin{aligned} F &= \left| \frac{\int_0^t 2G(t') e^{-\gamma_r t'} \tilde{G}^{-2}(0, t') dt'}{2 - \int_0^t 2G(t') e^{-\gamma_r t'} \tilde{G}^{-2}(0, t') dt'} \right| \\ &= \left| \frac{\int_1^{\text{final}} e^{-\gamma_r t'} d\left[\tilde{G}^{-2}(0, t')\right]}{2 + \int_1^{\text{final}} e^{-\gamma_r t'} d\left[\tilde{G}^{-2}(0, t')\right]} \right|. \end{aligned} \quad (52)$$

Although the above expression looks rather complicated, one important result can be seen relatively straightforwardly. The only difference between this expression and the one that would be obtained in the absence of decoherence is the factor $e^{-\gamma_r t'}$. This factor represents the rather intuitive fact that the parts in the QPC signal that are recorded at later times carry less value for purposes of determining the initial qubit state than those recorded at earlier times, with an exponentially decaying function. What is less intuitively obvious is how the exponential-decay function enters into the expression for the fidelity, as can be seen from equation (52).

It is worth making a comment here regarding the ‘value’ of the output signal in the absence of decoherence. One might be tempted to say that since the fidelity increase slows down as time goes by (see figure 3), the ‘value’ of the QPC’s output signal decreases as time goes by in that case as well. If that were the case, this decrease in the ‘value’ of the measurement signal would not be related to decoherence. However, one can see that this is not the case by considering the simple case $\beta = 0$ in the absence of decoherence. In that case the important quantity is the time-averaged QPC current throughout the measurement duration, without any weight function that decreases in time. All parts of the signal are therefore given equal importance when extracting the measurement result.

In order to calculate the average measurement fidelity in the presence of decoherence, one must average the measurement fidelity over all different input states and measurement outcomes. Since any calculation involving the above expressions seems to be a daunting task, we use the

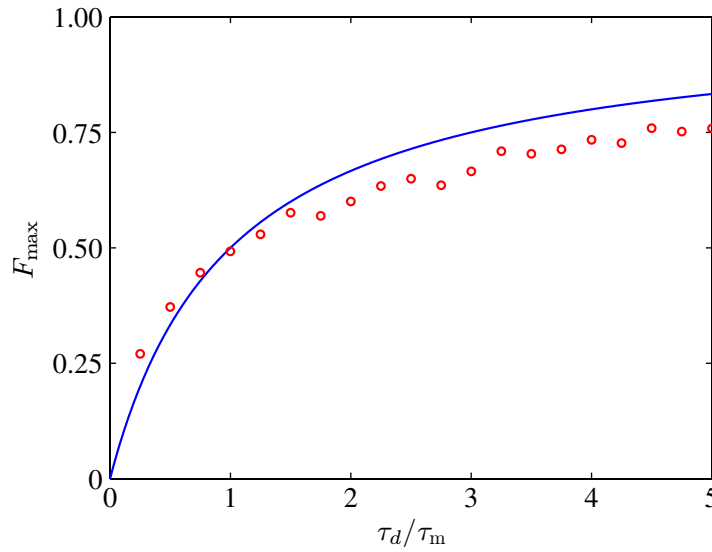


Figure 8. The maximum achievable fidelity as a function of the ratio between the decoherence and measurement times. The red dots are obtained using numerical simulations, and the solid line is given by equation (55).

following hand-waving calculation. In the absence of decoherence, the measurement fidelity after duration t can be expressed as

$$\begin{aligned}
 F(t) &\approx 1 - \exp\left\{-\frac{t}{\tau_m}\right\} \\
 &= \int_0^t \frac{1}{\tau_m} e^{-t/\tau_m} dt.
 \end{aligned} \tag{53}$$

Decoherence reduces the ‘value’ of the later parts of the measurement record with an exponentially decaying function (with characteristic time τ_d). An estimate for the average fidelity in the presence of decoherence can therefore be given in the form

$$F(t) \approx \int_0^t \frac{1}{\tau_m} e^{-t/\tau_m} \times e^{-t/\tau_d} dt. \tag{54}$$

Even if the measurement time is taken to infinity, where we have $F \rightarrow 1$ in the absence of decoherence, we find that the fidelity only reaches the value

$$F_{\max} = \frac{\tau_d}{\tau_m + \tau_d}. \tag{55}$$

Note, in particular, the simple limits that $F_{\max} \rightarrow 0$ when $\tau_d \ll \tau_m$, and $F_{\max} \rightarrow 1$ when $\tau_d \gg \tau_m$. We have performed numerical simulations of the measurement process in the presence of relaxation, and the results are shown in figure 8. The results agree reasonably well with those of the hand-waving argument given above.

6. Conclusion

In conclusion, we have analyzed the question of what information can be extracted from the output signal of a detector that weakly probes the state of a qubit when the qubit Hamiltonian

induces oscillations between the two eigenstates of the probed operator. We have shown that the measurement basis is determined stochastically every time the measurement is repeated. In the case of weak qubit–detector coupling, the possible measurement bases cover all the possible directions. The measurement basis and the measurement result can both be extracted from the detector’s output signal. We have also shown that the information acquisition rate is almost independent of the angle β between the direction defining the probed basis and that defining the qubit Hamiltonian. In other words, given enough time, the detector will produce a high-fidelity measurement result, regardless of the value of β . These results show that, under suitable conditions and by proper analysis, the detector’s ability to obtain high-fidelity information about the state of the qubit is not affected by the apparent conflict between the measurement and coherent-precession dynamics.

In the course of our analysis, we have introduced an equation that supplements the stochastic master equation for purposes of extracting measurement information from the observed signal. We have also introduced a procedure for performing quantum state tomography that is well suited for the case where the different measurement bases do not have a simple relation to one another.

We have outlined the generalization of our analysis to the case where the qubit experiences additional, non-measurement-related decoherence. In this case, the ‘value’ of the detector’s output signal decreases with the time at which it is recorded. We have demonstrated this fact by analyzing the case where the measurement is performed in the presence of relaxation.

Acknowledgments

We would like to thank D Burgarth, J R Johansson, N Lambert and A J Leggett for useful discussions. This work was supported in part by the National Security Agency (NSA), the Laboratory for Physical Sciences (LPS), the Army Research Office (ARO) and the National Science Foundation (NSF) grant no. EIA-0130383. JQY was also supported by the National Basic Research Program of China grant no. 2009CB929300, the National Natural Science Foundation of China grant no. 10625416, and the MOST International Collaboration Program grant no. 2008DFA01930.

Appendix A. The QPC-current probability distribution for a short time interval of size δt

In this appendix, we derive the expression for the probability distribution $P[I, \delta I, \delta t]$ that governs the stochastically determined values of the QPC current I . We use the discretization parameters δI and δt : δI defines the size of a finite interval of values for I that we identify with a single value of I , and δt is the size of the time interval under consideration. In the derivation below, we assume that the qubit is in one of its charge states (for definiteness $|L\rangle$) and that there is no mixing between the charge states. We denote the average value of the current by \bar{I}_L for the state $|L\rangle$ and \bar{I}_R for the state $|R\rangle$. We are assuming that the probability distribution can be approximated by a Gaussian distribution function:

$$P_L[I, \delta I, \delta t] \propto \exp \left\{ -\alpha (I - \bar{I}_L)^2 \right\}. \quad (\text{A.1})$$

In order to determine how δt enters in the expression for $P_L[I, \delta I, \delta t]$ we consider the effect of performing N measurements in a row. For sufficiently small δt , the results of any calculation

should not depend on whether we treat these measurements as N independent measurements or as a single measurement of length $N\delta t$. Since the values of I obtained in the different measurements are independent, their average will have a standard deviation σ/\sqrt{N} , where σ is the standard deviation of I for an interval of length δt . In other words, the standard deviation in I must be proportional to $1/\sqrt{\delta t}$. Since the coefficient α in equation (A.1) is related to the standard deviation σ by $\sigma = 1/\sqrt{2\alpha}$, we find that α must be proportional to δt : $\alpha = \tilde{\alpha}\delta t$.

We now introduce the measurement time τ_m by requiring that if δt were to reach τ_m , the standard deviations (or in other words, the widths) of the probability distributions $P_L[I, \delta I, \delta t]$ and $P_R[I, \delta I, \delta t]$ will be equal to half the distance between their center points: $1/\sqrt{2\tilde{\alpha}\tau_m} = |\bar{I}_R - \bar{I}_L|/2$. Note that this definition does not necessarily agree with other definitions of the measurement time that appear in the literature. Assuming for definiteness that $\bar{I}_R > \bar{I}_L$ and defining $\Delta\bar{I} = \bar{I}_R - \bar{I}_L$, we find that $\tilde{\alpha} = 2/(\tau_m[\Delta\bar{I}]^2)$. Using the normalization $\sum_I P_L[I, \delta I, \delta t] = \int P_L[I, \delta I, \delta t]dI/(\delta I) = 1$, we find that

$$P_L[I, \delta I, \delta t] = \sqrt{\frac{2\delta t (\delta I)^2}{\pi \tau_m (\Delta\bar{I})^2}} \exp\left\{-\frac{2\delta t (I - \bar{I}_L)^2}{\tau_m (\Delta\bar{I})^2}\right\}. \quad (\text{A.2})$$

This expression is used for deriving the matrices $U_M[I, \delta I, \delta t]$ in the main text of the paper.

Appendix B. The relation between a given output signal and its ‘opposite’

In this appendix, we would like to establish the relation between the measurement results of a certain signal and its ‘opposite’. If a signal is given by $I_1(t)$, with the time t running from 0 to t_f , the opposite signal is given by $I_2(t) = \bar{I} - I_1(t)$. In other words, the opposite signal is obtained by taking the mirror image of the signal about the central current value \bar{I} . We start by stating the relation: if

$$\hat{U}_{\text{Total}}[I_1(t : 0 \rightarrow t_f), \delta I, \delta t] = \hat{U}_{\text{Rot}}[I_1(t : 0 \rightarrow t_f), \delta I, \delta t] \times \hat{U}_{\text{Meas}}[I_1(t : 0 \rightarrow t_f), \delta I, \delta t], \quad (\text{B.1})$$

with

$$\hat{U}_{\text{Meas}}[I_1(t : 0 \rightarrow t_f), \delta I, \delta t] = \sqrt{P_1}|\psi_1\rangle \langle\psi_1| + \sqrt{P_2}|\psi_2\rangle \langle\psi_2|, \quad (\text{B.2})$$

then

$$\hat{U}_{\text{Total}}[I_2(t : 0 \rightarrow t_f), \delta I, \delta t] = \hat{U}_{\text{Rot}}[I_2(t : 0 \rightarrow t_f), \delta I, \delta t] \times \hat{U}_{\text{Meas}}[I_2(t : 0 \rightarrow t_f), \delta I, \delta t], \quad (\text{B.3})$$

with

$$\hat{U}_{\text{Meas}}[I_2(t : 0 \rightarrow t_f), \delta I, \delta t] = \sqrt{P_1}|\psi_2\rangle \langle\psi_2| + \sqrt{P_2}|\psi_1\rangle \langle\psi_1|, \quad (\text{B.4})$$

and $\hat{U}_{\text{Rot}}[I_2(t : 0 \rightarrow t_f), \delta I, \delta t] = \hat{U}_{\text{Rot}}[I_1(t : 0 \rightarrow t_f), \delta I, \delta t]$.

For $t_f = 0$, both $\hat{U}_{\text{Total}}[I_1(t : 0 \rightarrow t_f), \delta I, \delta t]$ and $\hat{U}_{\text{Total}}[I_2(t : 0 \rightarrow t_f), \delta I, \delta t]$ are given by the unit matrix, which obeys the relation given above. We now assume that the relation holds for a given value of t_f , and we try to establish that it will continue to hold at an infinitesimally later time $t_f + \delta t$. The two changes that can occur during this infinitesimal interval are a measurement-induced weak projection or a Hamiltonian-induced unitary transformation. Since $\hat{U}_{\text{Rot}}[I_2(t : 0 \rightarrow t_f), \delta I, \delta t] = \hat{U}_{\text{Rot}}[I_1(t : 0 \rightarrow t_f), \delta I, \delta t]$, application of $\exp\{-i\hat{H}\delta t\}$ to $\hat{U}_{\text{Total}}[I_1(t : 0 \rightarrow t_f), \delta I, \delta t]$ and $\hat{U}_{\text{Total}}[I_2(t : 0 \rightarrow t_f), \delta I, \delta t]$ clearly cannot affect the above relation between the total evolution matrices. Demonstrating that application of the weak projection also does not

affect the relation is less straightforward. Using equation (10) and introducing the (infinitesimal) quantity $q = \delta t[I_1(t_f) - \bar{I}]/(\tau_m \Delta \bar{I})$, we find that

$$\begin{aligned} \hat{U}_{\text{Total}}[I_1(t : 0 \rightarrow t_f + \delta t), \delta I, \delta t] &\propto (1 + q\hat{\sigma}_{\mathbf{n}}) \times \hat{U}_{\text{Rot}}[I_1(t : 0 \rightarrow t_f), \delta I, \delta t] \\ &\times \left(\sqrt{P_1}|\psi_2\rangle \langle\psi_2| + \sqrt{P_2}|\psi_1\rangle \langle\psi_1| \right) = \hat{U}_{\text{Rot}}[I_1(t : 0 \rightarrow t_f), \delta I, \delta t] \\ &\times (1 + q\hat{\sigma}_{\mathbf{n}}) \left(\sqrt{P_1}|\psi_2\rangle \langle\psi_2| + \sqrt{P_2}|\psi_1\rangle \langle\psi_1| \right), \end{aligned} \quad (\text{B.5})$$

where

$$\hat{\sigma}_{\mathbf{n}} = \hat{U}_{\text{Rot}}^\dagger[I_1(t : 0 \rightarrow t_f), \delta I, \delta t] \times (1 + q\hat{\sigma}_{\mathbf{n}}) \times \hat{U}_{\text{Rot}}[I_1(t : 0 \rightarrow t_f), \delta I, \delta t]. \quad (\text{B.6})$$

We now introduce the Pauli matrices $\tilde{\sigma}_z = |\psi_1\rangle \langle\psi_1| - |\psi_2\rangle \langle\psi_2|$ and $\tilde{\sigma}_x$, for which $q\hat{\sigma}_{\mathbf{n}} = q_x\tilde{\sigma}_x + q_z\tilde{\sigma}_z$. Defining $a_p = (\sqrt{P_1} + \sqrt{P_2})/2$ and $a_m = (\sqrt{P_1} - \sqrt{P_2})/2$, we find that

$$\begin{aligned} \hat{U}_{\text{Total}}[I_1(t : 0 \rightarrow t_f + \delta t), \delta I, \delta t] &\propto \hat{U}_{\text{Rot}}[I_1(t : 0 \rightarrow t_f), \delta I, \delta t] \times (1 + q_x\tilde{\sigma}_x + q_z\tilde{\sigma}_z) \times (a_p + a_m\tilde{\sigma}_z) \\ &= \hat{U}_{\text{Rot}}[I_1(t : 0 \rightarrow t_f), \delta I, \delta t] \times (a_p + a_p q_x\tilde{\sigma}_x + a_p q_z\tilde{\sigma}_z + a_m\tilde{\sigma}_z - ia_m q_x\tilde{\sigma}_y + a_m q_z) \\ &= \hat{U}_{\text{Rot}}[I_1(t : 0 \rightarrow t_f), \delta I, \delta t] \times \exp\{-ia_m q_x\tilde{\sigma}_y/a_p\} \\ &\times \left([a_p + a_m q_z] + \left[a_p q_x - \frac{a_m^2 q_x}{a_p} \right] \tilde{\sigma}_x + [a_m + a_p q_z]\tilde{\sigma}_z \right) + O(q^2) \\ &= \hat{U}_{\text{Rot}}[I_1(t : 0 \rightarrow t_f + \delta t), \delta I, \delta t] \times \hat{U}_{\text{Meas}}[I_1(t : 0 \rightarrow t_f + \delta t), \delta I, \delta t], \end{aligned} \quad (\text{B.7})$$

where

$$\begin{aligned} \hat{U}_{\text{Rot}}[I_1(t : 0 \rightarrow t_f + \delta t), \delta I, \delta t] &= \hat{U}_{\text{Rot}}[I_1(t : 0 \rightarrow t_f), \delta I, \delta t] \times \exp\{-ia_m q_x\tilde{\sigma}_y/a_p\}, \\ \hat{U}_{\text{Meas}}[I_1(t : 0 \rightarrow t_f + \delta t), \delta I, \delta t] &= a'_p + a'_{m,x}\tilde{\sigma}_x + a'_{m,z}\tilde{\sigma}_z, \\ a'_p &= a_p + a_m q_z, \\ a'_{m,x} &= a_p q_x - \frac{a_m^2 q_x}{a_p}, \\ a'_{m,z} &= a_m + a_p q_z. \end{aligned} \quad (\text{B.8})$$

We can now carry out the same derivation as above for the ‘opposite’ signal. The only changes are that we replace q by $-q$ (therefore replacing q_x by $-q_x$ and q_z by $-q_z$) and reverse the positions of P_1 and P_2 (this latter change changes a_m into $-a_m$ and leaves a_p unchanged). These changes leave the infinitesimal rotation angle $a_m q_x/a_p$ unchanged, and we therefore find that the relation $\hat{U}_{\text{Rot}}[I_2(t : 0 \rightarrow t_f + \delta t), \delta I, \delta t] = \hat{U}_{\text{Rot}}[I_1(t : 0 \rightarrow t_f + \delta t), \delta I, \delta t]$ holds. Similarly a'_p is unaffected by the above changes. The quantities $a'_{m,x}$ and $a'_{m,z}$, on the other hand, change their signs. By looking at the expressions for the a_p and a_m in terms of the P_1 and P_2 above, we can see that reversing the sign of a_m reverses the positions of the symbols P_1 and P_2 in the matrix \hat{U}_{Meas} , which is exactly the difference between $\hat{U}_{\text{Meas}}[I_1(t : 0 \rightarrow t_f + \delta t), \delta I, \delta t]$ and $\hat{U}_{\text{Meas}}[I_2(t : 0 \rightarrow t_f + \delta t), \delta I, \delta t]$ that was stated at the beginning of this appendix. We have thus established the relation between the matrices $\hat{U}_{\text{Total}}[I_1(t : 0 \rightarrow t_f), \delta I, \delta t]$ and $\hat{U}_{\text{Total}}[I_2(t : 0 \rightarrow t_f), \delta I, \delta t]$.

Appendix C. The measurement fidelity for two consecutive weak measurements

In this appendix, we show that the measurement fidelity for two misaligned weak measurements can be higher than that obtained when the measurement axes of the two measurements are aligned with each other⁷.

With no loss of generality, we take the measurement axis of the first measurement to be the z -axis (i.e. the basis $\{|0\rangle, |1\rangle\}$). We assume that the measurement produces one of two possible outcomes. The measurement matrices can therefore be expressed as

$$\begin{aligned}\hat{U}_{1,1} &= \begin{pmatrix} \sqrt{R_1(1+\epsilon_1)} & 0 \\ 0 & \sqrt{R_1(1-\epsilon_1)} \end{pmatrix}, \\ \hat{U}_{1,2} &= \begin{pmatrix} \sqrt{1-R_1(1+\epsilon_1)} & 0 \\ 0 & \sqrt{1-R_1(1-\epsilon_1)} \end{pmatrix},\end{aligned}\tag{C.1}$$

where we have neglected any coherent component in the measurement matrix, as explained in the main text. The above matrices satisfy the basic requirement that $\hat{U}_{1,1}^\dagger \hat{U}_{1,1} + \hat{U}_{1,2}^\dagger \hat{U}_{1,2} = 1$. The second measurement is performed in the basis $\{\cos(\theta/2)|0\rangle + \sin(\theta/2)|1\rangle, \sin(\theta/2)|0\rangle - \cos(\theta/2)|1\rangle\}$. The corresponding measurement matrices are given by

$$\begin{aligned}\hat{U}_{2,1} &= \sqrt{R_2(1+\epsilon_2)} \begin{pmatrix} \cos^2 \frac{\theta}{2} & \sin \frac{\theta}{2} \cos \frac{\theta}{2} \\ \sin \frac{\theta}{2} \cos \frac{\theta}{2} & \sin^2 \frac{\theta}{2} \end{pmatrix} \\ &\quad + \sqrt{R_2(1-\epsilon_2)} \begin{pmatrix} \sin^2 \frac{\theta}{2} & -\sin \frac{\theta}{2} \cos \frac{\theta}{2} \\ -\sin \frac{\theta}{2} \cos \frac{\theta}{2} & \cos^2 \frac{\theta}{2} \end{pmatrix}, \\ \hat{U}_{2,2} &= \sqrt{1-R_2(1+\epsilon_2)} \begin{pmatrix} \cos^2 \frac{\theta}{2} & \sin \frac{\theta}{2} \cos \frac{\theta}{2} \\ \sin \frac{\theta}{2} \cos \frac{\theta}{2} & \sin^2 \frac{\theta}{2} \end{pmatrix} \\ &\quad + \sqrt{1-R_2(1-\epsilon_2)} \begin{pmatrix} \sin^2 \frac{\theta}{2} & -\sin \frac{\theta}{2} \cos \frac{\theta}{2} \\ -\sin \frac{\theta}{2} \cos \frac{\theta}{2} & \cos^2 \frac{\theta}{2} \end{pmatrix}.\end{aligned}\tag{C.2}$$

The combined measurement has four possible measurement matrices, each one corresponding to one of the four possible outcomes. For example, for the outcome identified with the index 1 in both measurements, the measurement matrix is given by $\hat{U}_{2,1} \hat{U}_{1,1}$. In order to obtain the measurement fidelity for this outcome, we need to consider the matrix

$$\begin{aligned}\hat{U}_{1,1}^\dagger \hat{U}_{2,1}^\dagger \hat{U}_{2,1} \hat{U}_{1,1} &= \begin{pmatrix} \sqrt{R_1(1+\epsilon_1)} & 0 \\ 0 & \sqrt{R_1(1-\epsilon_1)} \end{pmatrix} \begin{pmatrix} R_2 + \epsilon_2 \cos \theta & \frac{R_2 \epsilon_2 \sin \theta}{2} \\ \frac{R_2 \epsilon_2 \sin \theta}{2} & R_2 - \epsilon_2 \cos \theta \end{pmatrix} \\ &\quad \times \begin{pmatrix} \sqrt{R_1(1+\epsilon_1)} & 0 \\ 0 & \sqrt{R_1(1-\epsilon_1)} \end{pmatrix}.\end{aligned}\tag{C.3}$$

⁷ For a study on a related subject, see Wei and Nazarov [21]. A somewhat related experimental study is given in Deppe *et al* [21].

If we denote the eigenvalues of this matrix by P_1 and P_2 (with $P_1 > P_2$), the measurement fidelity for this outcome is given by $(P_1 - P_2)/(P_1 + P_2)$. For purposes of calculating the overall fidelity of the measurement sequence, we take the maximally mixed state,

$$\rho_{\text{max. mixed}} = \begin{pmatrix} \frac{1}{2} & 0 \\ 0 & \frac{1}{2} \end{pmatrix} \quad (\text{C.4})$$

as the initial state. With this initial state, the probability that the above outcome is obtained in a given experimental run is given by $(P_1 + P_2)/2$. Thus, the overall fidelity (taking into account all four possible outcomes) will be given by the sum of four terms, each of which is given by $(P_1 - P_2)/2$ for one of the possible outcomes. For equation (C.3) straightforward algebra gives the result that

$$\frac{P_1 - P_2}{2} = R_1 R_2 \sqrt{(1 + \epsilon_1 \epsilon_2 \cos \theta)^2 - (1 - \epsilon_1^2)(1 - \epsilon_2^2)}. \quad (\text{C.5})$$

Similar expressions can be obtained for the three other possible outcomes, resulting in the overall fidelity

$$\begin{aligned} F = & R_1 R_2 \sqrt{(1 + \epsilon_1 \epsilon_2 \cos \theta)^2 - (1 - \epsilon_1^2)(1 - \epsilon_2^2)} + R'_1 R_2 \sqrt{(1 + \epsilon'_1 \epsilon_2 \cos \theta)^2 - (1 - \epsilon_1'^2)(1 - \epsilon_2^2)} \\ & + R_1 R'_2 \sqrt{(1 + \epsilon_1 \epsilon'_2 \cos \theta)^2 - (1 - \epsilon_1^2)(1 - \epsilon_2'^2)} \\ & + R'_1 R'_2 \sqrt{(1 + \epsilon'_1 \epsilon'_2 \cos \theta)^2 - (1 - \epsilon_1'^2)(1 - \epsilon_2'^2)}, \end{aligned} \quad (\text{C.6})$$

where $R'_j = 1 - R_j$ and $\epsilon'_j = -\epsilon_j R_j / (1 - R_j)$.

The measurement fidelity can have its maximum at any point between zero and π (with the proper choice of the parameters R_j and ϵ_j ; we have verified this statement numerically). For the special case $R_1 = R_2 = 1/2$ and $\epsilon_1 = \epsilon_2 \equiv \epsilon > 0$, the overall measurement fidelity is given by

$$F = \frac{1}{2} \left(\sqrt{(1 + \epsilon^2 \cos \theta)^2 - (1 - \epsilon^2)^2} + \sqrt{(1 - \epsilon^2 \cos \theta)^2 - (1 - \epsilon^2)^2} \right). \quad (\text{C.7})$$

Differentiating this expression twice shows that it has a maximum at $\cos \theta = 0$. In fact, in the limit of weak measurement, i.e. $\epsilon \ll 1$, one can see easily that the above expression can be approximated by

$$F \approx \epsilon \left(\left| \cos \frac{\theta}{2} \right| + \left| \sin \frac{\theta}{2} \right| \right), \quad (\text{C.8})$$

which has minima at $\theta = 0$ and $\theta = \pi$ ($F = \epsilon$) and a maximum at $\theta = \pi/2$ ($F = \sqrt{2}\epsilon$). The relative difference between the minimum and maximum fidelities is approximately 30%.

The result that the fidelity of two weak measurement can be enhanced when they are not aligned with one another offers some explanation for the result of section 4 that the fidelity increases more rapidly when the qubit Hamiltonian and the probed operator do not commute. The qubit Hamiltonian causes a rotation in the qubit's state, while the state is being measured along a fixed axis. This situation is, in some sense, equivalent to one where a number of different qubit operators are sequentially probed.

A final comment that is worth making here regards the possible bases of the combined measurement. As can be seen from the analysis of this appendix, when the two performed

measurements correspond to directions in the x - z -plane, all the resulting matrices will be real. As a result, all the possible effective measurements will be in the x - z -plane as well (note that a projector along the y -axis would be complex). In other words, when successive measurements are made in one plane, they can only result in effective measurements made in the same plane. This result explains why in the special case $\beta = \pi/2$ all the possible measurement bases lay in the x - y -plane; successive measurements along the x -axis separated by state precession about the z -axis are equivalent to a sequence of measurements that are all performed in the x - y -plane.

Appendix D. Quantum state tomography

In this appendix, we derive the function that was used to perform quantum state tomography in section 4.

We start with the objective of performing quantum state tomography using the available measurement data, which we assume has been obtained using a (generally weakly coupled) QPC as explained in the main text. We note that since the measurements in the different experimental runs are generally performed in different bases, we look for a procedure that treats all the measurements on equal footing and does not have a preferred measurement basis, or set of bases. One obvious approach to follow is to construct a function that assigns a penalty for any deviation by the ‘guess’ density matrix ρ_{guess} from a given experimental result (which takes the form of a measured, pure state). The guess density matrix is characterized by the spherical coordinates r_{guess} , θ_{guess} and ϕ_{guess} , whereas the measured state is characterized by only the angles in spherical coordinates θ_j and ϕ_j (the index j denotes the different experimental runs). The function to be minimized for purposes of state tomography will therefore have the form

$$\mathcal{T}(r_{\text{guess}}, \theta_{\text{guess}}, \phi_{\text{guess}}) = \sum_j f(r_{\text{guess}}, \theta_{\text{guess}}, \phi_{\text{guess}}, \theta_j, \phi_j). \quad (\text{D.1})$$

In order to proceed further, we now consider what is done in the standard version of state tomography where the average values $\langle \hat{\sigma}_x \rangle$, $\langle \hat{\sigma}_y \rangle$ and $\langle \hat{\sigma}_z \rangle$ are measured and the density matrix $\rho = (1 + \langle \hat{\sigma}_x \rangle \hat{\sigma}_x + \langle \hat{\sigma}_y \rangle \hat{\sigma}_y + \langle \hat{\sigma}_z \rangle \hat{\sigma}_z)/2$ is inferred from the measurement data. If we take the measurement data for $\hat{\sigma}_z$, we know that we want the tomography procedure to produce the result $r \cos \theta = (N_{+1} - N_{-1})/(N_{+1} + N_{-1})$, where N_{+1} and N_{-1} are the number of times that the measurement results $+1$ and -1 were obtained, respectively. We can therefore see that the function $f(r_{\text{guess}}, \theta_{\text{guess}}, \phi_{\text{guess}}, \theta_j = 0, \phi_j)$ will only be a function of $\langle \hat{\sigma}_{z, \text{guess}} \rangle = r_{\text{guess}} \cos \theta_{\text{guess}}$ (or, in other words, the projection of the vector representing the guess density matrix along the measurement axis). Taking this measurement data, we find that the function \mathcal{T} has the form:

$$\mathcal{T}(\langle \hat{\sigma}_{z, \text{guess}} \rangle, N_{+1}, N_{-1}) = N_{+1} f(\langle \hat{\sigma}_{z, \text{guess}} \rangle) + N_{-1} f(-\langle \hat{\sigma}_{z, \text{guess}} \rangle). \quad (\text{D.2})$$

In order to minimize the function \mathcal{T} , we take its derivative with respect to $\langle \hat{\sigma}_{z, \text{guess}} \rangle$:

$$\frac{d\mathcal{T}(\langle \hat{\sigma}_{z, \text{guess}} \rangle, N_{+1}, N_{-1})}{d\langle \hat{\sigma}_{z, \text{guess}} \rangle} = N_{+1} f'(\langle \hat{\sigma}_{z, \text{guess}} \rangle) - N_{-1} f'(-\langle \hat{\sigma}_{z, \text{guess}} \rangle). \quad (\text{D.3})$$

If we now use the Taylor expansion

$$f'(\langle \hat{\sigma}_{z, \text{guess}} \rangle) = \sum_{n=0}^{\infty} c_n \langle \hat{\sigma}_{z, \text{guess}} \rangle^n, \quad (\text{D.4})$$

we find that

$$\begin{aligned} \frac{d\mathcal{T}(\langle \hat{\sigma}_{z,\text{guess}} \rangle, N_{+1}, N_{-1})}{d\langle \hat{\sigma}_{z,\text{guess}} \rangle} &= \sum_{n=0,2,4,\dots} \left\{ (N_{+1} - N_{-1})c_n \langle \hat{\sigma}_{z,\text{guess}} \rangle^n + (N_{+1} + N_{-1})c_{n+1} \langle \hat{\sigma}_{z,\text{guess}} \rangle^{n+1} \right\} \\ &= (N_{+1} + N_{-1}) \sum_{n=0,2,4,\dots} \left\{ c_n \langle \hat{\sigma}_{z,\text{correct}} \rangle + c_{n+1} \langle \hat{\sigma}_{z,\text{guess}} \rangle \right\} \langle \hat{\sigma}_{z,\text{guess}} \rangle^n, \end{aligned} \quad (\text{D.5})$$

where $\langle \hat{\sigma}_{z,\text{correct}} \rangle = (N_{+1} - N_{-1}) / (N_{+1} + N_{-1})$. In order to ensure that the function \mathcal{T} has a minimum at $\langle \hat{\sigma}_{z,\text{guess}} \rangle = \langle \hat{\sigma}_{z,\text{correct}} \rangle$, we must choose $c_n = -c_{n+1}$ for every even number n . The simplest choice is $c_0 = -c_1 = -1/2$ and $c_2 = c_3 = \dots = 0$. This choice gives the function

$$\mathcal{T}(r_{\text{guess}}, \theta_{\text{guess}}, \phi_{\text{guess}}) = \sum_j [1 - \langle \hat{\sigma}_{z,\text{guess}} \rangle]^2, \quad (\text{D.6})$$

which, when generalized to the case where the measurement axis is not necessarily the z -axis, gives equation (37).

The detailed analysis of the different possible choices of c_n in the function \mathcal{T} , and the stability and reliability of these different choices, is beyond the scope of this paper.

References

- [1] Zurek W H 1991 *Phys. Today* **44** 36
Braginsky V and Khalili F Y 1995 *Quantum Measurement* (Cambridge: Cambridge University Press)
- [2] Nielsen M A and Chuang I L 2000 *Quantum Computation and Quantum Information* (Cambridge: Cambridge University Press)
- [3] Gurvitz S A 1997 *Phys. Rev. B* **56** 15215
Elattari B and Gurvitz S A 2000 *Phys. Rev. Lett.* **84** 2047
Gurvitz S A and Berman G P 2005 *Phys. Rev. B* **72** 073303
Gilad T and Gurvitz S A 2006 *Phys. Rev. Lett.* **97** 116806
- [4] Korotkov A N 1999 *Phys. Rev. B* **60** 5737
Korotkov A N 2001 *Phys. Rev. B* **63** 115403
Korotkov A N and Averin D V 2001 *Phys. Rev. B* **64** 165310
Averin D V and Sukhorukov E V 2005 *Phys. Rev. Lett.* **95** 126803
- [5] Makhlin Y, Schön G and Shnirman A 2000 *Phys. Rev. Lett.* **85** 4578
- [6] Goan H-S, Milburn G J, Wiseman H M and Sun H B 2001 *Phys. Rev. B* **63** 125326
- [7] Pilgram S and Büttiker M 2002 *Phys. Rev. Lett.* **89** 200401
- [8] Jordan A N and Büttiker M 2005 *Phys. Rev. B* **71** 125333
Jordan A N and Büttiker M 2006 *Phys. Rev. Lett.* **95** 220401
- [9] Johansson G, Tornberg L, Shumeiko V S and Wendin G 2006 *J. Phys.: Condens. Matter* **18** S901
- [10] Ouyang S H, Lam C H and You J Q 2006 *J. Phys.: Condens. Matter* **18** 11551
- [11] Reuther G M, Zueco D, Hänggi P and Kohler S 2009 *Phys. Rev. Lett.* **102** 033602
- [12] Clerk A A, Devoret M H, Girvin S M, Marquardt F and Schoelkopf R J 2008 arXiv:0810.4729
- [13] Romito A, Gefen Y and Blanter Y M 2008 *Phys. Rev. Lett.* **100** 056801
Shpitalnik V, Gefen Y and Romito A 2008 *Phys. Rev. Lett.* **101** 226802
- [14] Kurotani Y, Sagawa T and Ueda M 2007 *Phys. Rev. A* **76** 022325
Sagawa T and Ueda M 2008 *Phys. Rev. A* **77** 012313
Wei H and Nazarov Y V 2008 *Phys. Rev. B* **78** 045308
Lambert N and Nori F 2008 *Phys. Rev. B* **78** 214302

- [15] Sillanpää M A, Lehtinen T, Paila A, Makhlin Yu, Roschier L and Hakonen P J 2005 *Phys. Rev. Lett.* **95** 206806
Duty T, Johansson G, Bladh K, Gunnarsson D, Wilson C and Delsing P 2005 *Phys. Rev. Lett.* **95** 206807
Shevchenko S N, van der Ploeg S H W, Grajcar M, Il'ichev E, Omelyanchouk A N and Meyer H-G 2008 *Phys. Rev. B* **78** 174527
Il'ichev E, van der Ploeg S H W, Grajcar M and Meyer H G 2009 *Quantum Inf. Process.* **8** 133
- [16] Kreisbeck C, Kaiser F J and Kohler S 2009 arXiv:0904.2754
- [17] Jacobs K and Steck D A 2006 *Contemp. Phys.* **47** 279
Brun T 2002 *Am. J. Phys.* **70** 719
- [18] Ashhab S, You J Q and Nori F 2009 *Phys. Rev. A* **79** 032317
- [19] Ashhab S, Niskanen A O, Harrabi K, Nakamura Y, Picot T, de Groot P C, Harmans C J P M, Mooij J E and Nori F 2008 *Phys. Rev. B* **77** 014510
Fedichkin L, Shapiro M and Dykman M I 2009 *Phys. Rev. A* at press (arXiv:0903.0012)
- [20] D'Ariano G M, Paris M G A and Sacchi M F 2003 *Adv. Imaging Electron Phys.* **128** 205
- [21] Wei H and Nazarov Y V 2008 *Phys. Rev. B* **78** 045308
Deppe F, Mariani M, Menzel E P, Saito S, Kakuyanagi K, Tanaka H, Meno T, Semba K, Takayanagi H and Gross R 2007 *Phys. Rev. B* **76** 214503
- [22] Bengtsson I and Zyczkowski K 2006 *Geometry of Quantum States* (Cambridge: Cambridge University Press)